The esophageal epithelium in systemic sclerosis: cellular and molecular dysregulation revealed by single-cell RNA sequencing

Matthew Dapas[1], Margarette H. Clevenger[2], Hadijat M. Makinde[1], Tyler Therron[1], Dustin A. Carlson[2,3], Mary Carns[1], Kathleen Aren[1], Cenfu Wei[2], Lutfiyya N. Muhammad[4], Carrie L. Richardson[1], Monique Hinchcliff[5], John E. Pandolfino[2,3], Harris R. Perlman[1*], Deborah R. Winter[1*], Marie-Pier Tetreault[2*]

Affiliations:

1. Division of Rheumatology, Department of Medicine, Northwestern University Feinberg School of Medicine, Chicago, IL, USA
2. Division of Gastroenterology & Hepatology, Department of Medicine, Northwestern University Feinberg School of Medicine, Chicago, IL, USA
3. Kenneth C. Griffin Esophageal Center of Northwestern Medicine, Northwestern University Feinberg School of Medicine, Chicago, IL, USA
4. Department of Preventive Medicine, Northwestern University Feinberg School of Medicine, Chicago, IL, USA
5. Section of Rheumatology, Allergy & Immunology, Department of Medicine, Yale School of Medicine, New Haven, CT, USA

*These authors jointly supervised the work

ABSTRACT

Systemic sclerosis (SSc) is a rare autoimmune disease characterized by vasculopathy and progressive fibrosis of the skin and internal organs. Individuals with SSc often suffer from chronic acid reflux and dysphagia due to loss of esophageal motility. However, the pathogenesis of esophageal dysmotility in SSc is poorly understood. To determine whether distinct changes in esophageal epithelial cells contribute to impaired motility in SSc, we investigated the stratified squamous esophageal epithelium using single-cell RNA sequencing (n=306,372 cells) in individuals with SSc compared those with gastroesophageal reflux disease (GERD) as well as healthy controls. The proportion of epithelial cells in the outermost, superficial compartment of the esophageal epithelium was significantly reduced in SSc (9.4% vs 21.6% in HCs). Differential gene expression in SSc was primarily limited to the superficial compartment (3,572 genes vs. 232 in all other compartments), with significant upregulation of extracellular matrix and keratinization genes. These cellular and molecular changes in SSc were highly correlated with those seen in GERD, indicating they were secondary to reflux; however, their magnitudes were more pronounced in the proximal esophagus, suggesting that esophageal dysmotility leads to greater proximal acid exposure, which may contribute to aspiration. SSc-specific gene dysregulation implicated immunoregulatory pathways likely pertinent to pathogenic mechanisms. By offering a comprehensive view of transcriptional dysregulation at single-cell resolution in human esophageal epithelial cells in SSc compared to GERD and healthy tissue, this work clarifies the state of epithelial cells in SSc-induced esophageal dysfunction.

INTRODUCTION

Systemic sclerosis (SSc), also known as scleroderma, is an immune-mediated rheumatic disease of unknown etiology that causes progressive fibrosis of the skin and internal organs. Although uncommon (18-26 per 100,000 people)[1-4], SSc is one of the deadliest autoimmune disorders[5], with a 10-year survival rate of 45-68% following diagnosis[4,6,7]. Over 90% of individuals with SSc report gastrointestinal (GI) dysfunction[8], with esophageal dysmotility being the most common GI manifestation[9]. Individuals with SSc and esophageal involvement typically suffer from chronic acid reflux and dysphagia due to loss of esophageal motility and are at much greater risk of esophageal stricture and Barrett's esophagus[8,10,11]. The rate of esophageal involvement was nearly twice as high in individuals with SSc who died within 5 years of diagnosis[12].

There are multiple, interrelated mechanisms that may cause esophageal dysmotility in SSc. Vascular damage and neurogenic impairment lead to smooth muscle cell fibrosis[13], but esophageal muscle atrophy has also been observed in SSc without vasculopathy or fibrosis[14]. Inflammatory signatures[15], absence of anti-centromere antibodies[16], and presence of anti-topoisomerase I antibodies are associated with esophageal complications, as well[8]. Complicating research efforts is significant clinical and molecular heterogeneity observed between SSc patients[17-19] and difficulty distinguishing between effects from autoimmune processes and secondary factors such as severe reflux. Consequently, the pathogenesis of esophageal disease in SSc remains poorly understood.

Molecular investigations of SSc esophageal involvement have primarily focused on canonical pathways in submucosal and muscle layers[20]. However, the mucosa is no less essential for normal esophageal transport[21,22], and recent studies have suggested that esophageal epithelial cells (EECs) may play a more central role in the pathogenesis of SSc esophageal involvement than previously thought[20]. Mouse models with epithelial-cell-specific knockout of *Fli1*, an Ets transcription factor implicated in SSc pathogenesis[23], spontaneously develop dermal and esophageal fibrosis and interstitial lung disease[24]. Importantly, the resultant lung disease is mediated by T-cell autoimmunity, but fibrosis of the skin and

esophagus persist in mice additionally lacking mature T and B cells, suggesting that the fibrosis is principally driven by the epithelia[20,24].

Most studies implicating epithelial cells in SSc esophageal dysmotility have been performed in mice or *in vitro*, and molecular analyses in humans have so far been limited to bulk tissues[15]. Furthermore, single-cell gene expression studies performed in other diseases of the esophagus, including squamous cell carcinoma[25,26] and allergic eosinophilic esophagitis[27,28], have identified substantial cellular and molecular changes in EECs compared to healthy tissue, such as significant expansion of non-proliferative suprabasal cells[27,28]. Therefore, to comprehensively investigate the effects of SSc on the esophageal epithelium, we performed single-cell RNA sequencing (scRNA-seq) of esophageal mucosal biopsies from SSc patients with clinically significant esophageal involvement and compared EEC distributions and gene expression signatures to individuals with gastroesophageal reflux disease (GERD) and healthy controls (HCs). By examining gene expression profiles from human tissue at single-cell resolution, this work sheds essential light on the cellular roots of esophageal dysfunction in SSc by clarifying the pathogenic role of the squamous epithelium, one of the most integral tissues supporting healthy esophageal function.

METHODS

Subjects

The SSc study population were recruited from adult patients aged 18 to 89 diagnosed with SSc according to the 2013 ACR/EULAR classification criteria, who visited the Northwestern Medicine Esophageal Center for esophageal symptom evaluation and motility testing, as described previously[29], between 2020 and 2021. Patients with GERD were recruited at the primary visit following positive wireless pH testing[28]. Patients with technically inadequate panometry or manometry studies, previous foregut surgeries (including prior pneumatic dilation), or mechanical obstructions in the esophagus such as esophageal stricture, eosinophilic esophagitis, severe reflux esophagitis (Los Angeles classification C or D), or hiatal hernias larger than 5 cm were excluded. HCs met asymptomatic criteria including lack of esophageal symptoms, no history of

alcohol dependency or tobacco use, body mass index less than 30kg/m^2, and no current antacid or proton pump inhibitor treatment[28]. The study protocol received approval from the Northwestern University Institutional Review Board.

Symptom evaluation and motility testing

Esophageal function testing included functional lumen imaging probe (FLIP) panometry during sedated endoscopy, high-resolution manometry (HRM), and in some subjects, 24-hour pH-impedance or timed-barium esophagram, which were completed and interpreted as previously described[30-33]. HRM classifications were based on the application of the Chicago Classification v4.0 to 10 supine and 5 upright test swallows[34]. FLIP panometry classifications were based on previous evaluation of asymptomatic volunteers and patients[35-37]. During endoscopy (same encounter as FLIP), esophageal mucosal biopsies were obtained at approximately 5-cm ("distal esophagus") and 15-cm ("proximal esophagus") proximal to the squamocolumnar junction. Acid exposure was measured as the percentage of time with esophageal pH<4 over a monitoring period of 24 hours. Most patients also completed validated symptom-questionnaires (patient-reported outcomes) on the day of esophageal motility testing with FLIP or HRM, including the Brief Esophageal Dysphagia Questionnaire (BEDQ), the Gastroesophageal Reflux Disease Questionnaire (GerdQ), and the Northwestern esophageal quality of life (NEQOL) survey.[38-40].

Sample processing and sequencing

Esophageal mucosal biopsies from proximal and distal esophagus were processed for scRNA-seq as described in Clevenger et al[28]. Briefly, following tissue digestion and filtering, cell suspensions met 85% minimum viability via Cellometer Auto2000 (Nexcelom Bioscience). Cells were loaded into a Chromium iX controller (10X Genomics) on a Chromium Next GEM Chip G (10X Genomics) to capture approximately 10,000 cells per sample and were processed for encapsulation following the manufacturer's protocol. Cell barcoding and library construction were performed using the 10X Genomics Chromium Next GEM Single Cell 3' Reagents Kits v3.1 and Dual Index Kit TT Set A according to the manufacturer's

protocol. Sequencing was performed by the NUseq Core using the Illumina Novaseq 6000. Paired-end reads consisting of a 28-base-pair read for cell barcodes and unique molecular identifiers and a 90-base-pair read for transcripts were aligned to the GRCh38 reference transcriptome using Cell Ranger v6.1.2.

Sample and cell quality control

Samples with high ambient RNA (<70% of sequencing reads mapped to cells) were removed from consideration. Gene expression counts generated by Cell Ranger were analyzed using Seurat v4.3.0[41] in R v4.3.0. Cells with low gene diversity (<200 unique genes), low unique molecular identifier counts (<500), or excessive counts (>100,000) were removed from consideration. Cells with high proportions of mitochondrial DNA reads, indicative of apoptosis or lysis, were removed using the bivariate regression models implemented in the miQC package[42]. Cells were filtered if their proportion of reads mapped to mitochondrial DNA exceeded 0.05 and their posterior probability of belonging to a compromised cell distribution was greater than 0.75 according to miQC. Doublets, in which more than one cell is clumped together in a single droplet, were predicted and removed using scDblFinder[43] with an expected, additive doublet rate of 0.01 per thousand cells with standard deviation of 0.01.

Sample integration and cell type annotation

Individual samples were normalized and integrated on 3,000 variable features using Seurat's SCTransform procedure[44] with v2 regularization[45] and canonical correlation analysis dimension reduction. Integration anchors were determined using a reference consisting of three pairs of proximal and distal samples from HCs. Principal component (PC) analysis was performed on the transformed and integrated expression counts. Uniform manifold approximation and projection (UMAP)[46] embeddings were calculated on the top 40 PCs with n=200 neighbors. Cell clustering was performed using Seurat's modularity-based clustering on a shared nearest neighbor (SNN) graph with k=25 on the top 40 PCs. Clusters were annotated according to the expression of established cell-specific gene markers (**Supplemental Table 1**, **Supplemental Figure**

1). For annotation of smaller cell clusters, we first filtered out the epithelial, myeloid, lymphoid, and endothelial cell clusters and then recomputed PCs and re-clustered the subset (PCs = 25, k=15).

Epithelial cell characterization

After isolating the subset of epithelial cell clusters, we further filtered cells with disproportionately low read counts (≤3,500; **Supplemental Figure 2, A-C**). The samples were then re-integrated using the procedure described above. UMAP embeddings were calculated on the top 35 PCs with n=100 neighbors. Epithelial compartments (basal, suprabasal, and superficial) were identified according to expression of established markers (**Supplemental Figure 4D**)[27,28,47-50]. For each compartment, we computed composite gene signature scores using Seurat's AddModuleScore() function (**Supplemental Figure 2E**). Cells were initially clustered on an SNN graph with k=50 with resolution=0.25 (**Supplemental Figure 2F**), but because the modularity optimization clustering implemented in Seurat grouped proliferating cells across different epithelial compartments and inconsistently distinguished suprabasal and superficial cells, we applied K-means clustering on the expression of the compartment-specific markers to delineate epithelial compartments. We performed separate K=2 K-means clustering on 1) the Seurat clusters containing basal and early suprabasal cells (clusters 1-5) to distinguish basal from suprabasal compartments and 2) the Seurat clusters containing late suprabasal and superficial cells (clusters 6-8) to demarcate suprabasal and superficial compartments (**Supplemental Figure 2, G-H**). Proliferating epithelial cells were identified using Seurat's CellCycleScoring() function. Cells predicted as being in S or G2/M phases based on the relative expression of corresponding markers[51] were labeled as proliferating cells (**Supplemental Figure 2I**). We tested for statistical differences in proportions of epithelial cell populations between conditions using MASC[52]. To derive a continuous epithelial differentiation score for each cell (**Supplemental Figure 3**), we combined the compartment-specific module scores as follows :

$$EDS_C = score_{suprabasal} + score_{superficial} - score_{basal}$$

Where EDS_C is the epithelial differentiation score for a given cell. This EDS_C was then scaled between 0 and 1:

$$EDS_{C,scaled} = \frac{EDS_C - \min(EDS_1, \ldots, EDS_n)}{\max(EDS_1, \ldots, EDS_n) - \min(EDS_1, \ldots, EDS_n)}$$

Gene expression analysis

To identify dysregulated pathways in SSc, we first calculated differential gene expression between conditions within each epithelial compartment, considering each cell as a sample. Differential gene expression was calculated using the FindMarkers() function in Seurat with the Wilcoxon rank-sum test on log-normalized RNA counts for genes expressed in at least 1% of cells by compartment. We adjusted for multiple testing using a Bonferroni correction accounting for the number of genes tested. Genes with an adjusted $P<0.05$ and absolute $\log_2$ fold change >0.1 were considered significantly differentially expressed. [53,54] Genes were then ranked by the magnitude and statistical certainty of their expression differences:

$$Weight = -\log_{10}(p) * abs(\log_2[FC])$$

Gene set enrichment was calculated using 3,795 canonical pathway gene sets from the Human Molecular Signatures Database[55] using gene set enrichment analysis (GSEA)[53,54]. Statistical gene set enrichment was calculated using one-way positive enrichment with 100,000 permutations on pathways with at least 10 genes. Mitochondrial and ribosomal genes were excluded from the GSEA.

To more robustly characterize gene expression differences between conditions[56], we performed pseudo-bulk differential expression analysis by aggregating RNA counts per sample within epithelial compartments. Genes with at least one count per million detected in at least 75% of samples in at least one condition per epithelial compartment were analyzed. To mitigate outlier-driven signals, genes with log-transformed expression greater than 3 standard deviations from the mean in exactly one individual were

197 excluded. Differential gene expression was evaluated using edgeR v3.42.4[57-59]. Gene expression was
198 modeled using a quasi-likelihood negative binomial generalized linear model, with global negative-
199 binomial trended dispersion estimated across all samples and gene-specific quasi-likelihood dispersions
200 estimated within each epithelial compartment. Differences in gene expression across conditions were
201 assessed using quasi-likelihood F-tests with false-discovery rate (FDR) adjustment. We conducted tests
202 combining both proximal and distal esophageal regions, as well as separate tests for each esophageal region.
203 Transcription factor enrichment analyses were conducted on the pseudo-bulk results using the
204 enricher() function from clusterProfiler v4.8.3[60]. We used consensus results from ENCODE[61] and ChEA[62],
205 as curated by the Ma'ayan Lab[63] and available at http://amp.pharm.mssm.edu/Enrichr/[64]to test for the
206 enrichment of transcription factor target genes from among genes that were differentially expressed
207 between SSc, GERD, and HCs with Bonferroni-adjusted $p<0.05$. Background gene sets were comprised of
208 the genes included in the pseudo-bulk differential expression analyses for each epithelial compartment.
209 Transcription factors absent from the background gene set were removed as candidate transcription factors.
210 Separate enrichment tests were performed for all differentially expressed genes (DEGs) and those that were
211 upregulated or downregulated in SSc. Enrichment results were adjusted using a Bonferroni correction
212 accounting for the number of transcription factors with more than 2 genes in the significant DEG list .
213
214 **Pseudo-bulk sample permutation**
215 Because of the sample size imbalance by disease state, which inherently yields different statistical power
216 for different tests across conditions, we permuted differential expression testing with equivalent sample
217 sizes to better evaluate the relative extent of dysregulation by EEC compartment and biopsy location
218 between SSc and GERD. We permuted all possible combinations of SSc samples with sample size n=4 for
219 both the proximal and distal regions and used the median statistics in the SSc vs. HCs tests to more directly
220 compare the results with those observed in GERD vs. HCs.
221
222 **Gene expression trajectory analysis**

To model gene expression as a continuous function along the axis of epithelial cell differentiation, we utilized the framework implemented in Lamian[65], with the epithelial differentiation score serving as the underlying pseudotime metric. Lamian fits a polynomial B-spline curve with the number of knots determined by minimization of the Bayesian Information Criterion. With few cells near the lower and upper limits of our epithelial differentiation score and the interpolation range bound by the minimum and maximum pseudotime values, the B-spline models produced erratic fits near the interpolation boundaries. Therefore, we instead modeled natural cubic splines, which are constrained to linearity at the boundaries (second derivative is zero), and we excluded the lowest and highest 1% of cells from the interpolation interval. Using these modeled gene expression trajectories, we performed hierarchical clustering of differential gene trajectories for all genes that were significantly differentially expressed between SSc and HC in single-cell-level differential expression testing.

Clinical phenotype associations

To test for associations with categorical measures of esophageal function (FLIP, HRM, and a combined FLIP and HRM with NeuroMyogenic [NM] classification[66]), we performed ordinal logistic regression that modeled likelihoods of increasing clinical severity. We excluded individuals with achalasia or esophagogastric junction outflow obstruction (EGJOO) from ordinal regression modeling motility. For FLIP we combined the "borderline/diminished" and "impaired/disordered" phenotypes. For NM we combined the Stage I and Stage II ineffective motility phenotypes. The resultant ordering for the ordinal regression was "normal"< "ineffective" < "absent" for HRM; "normal" < "borderline/diminished & impaired/disordered" < "absent" for FLIP; and "normal" < "stages I & II – ineffective" < "stage III – absent" for NM.

For association testing with quantitative clinical measures in SSc, we first performed a principal components analysis (PCA) on a set of nine quantitative clinical traits: HRM mean distal contractile interval (DCI), HRM basal esophagogastric junction (EGJ) pressure, HRM EGJ contractile index, HRM median integrated relaxation pressure (IRP), FLIP intra-balloon pressure at 60ml, FLIP EGJ distensibility index,

the GerdQ impact score, the BEDQ score, and the NEQOL score. Missing values were imputed with the mean. We then modeled associations with the first two PCs using linear regression. Gene expression was represented using log-transformed counts.

RESULTS

Whole tissue single-cell RNA sequencing (scRNA-seq) was performed on paired proximal and distal mucosal biopsies from ten patients with systemic sclerosis (SSc), four with gastroesophageal reflux disease (GERD), and six healthy controls (HCs). All participants but one in each group were female (**Table 1**). SSc patients were significantly older than HCs (54.9 vs 27.0 years; P<0.001). Among SSc patients, six had the limited cutaneous subtype, three had the diffuse cutaneous subtype, and one had sine scleroderma with no cutaneous symptoms (**Supplemental Table 1**). Mean SSc disease duration at the time of biopsy was 132 months. All SSc patients had positive serum antinuclear antibody and impaired esophageal motility. Following sample-level quality control (**Supplemental Table 2**), 39 samples were retained for analysis, including 19 from the proximal esophagus and 20 from the distal esophagus.

Characterization of esophageal mucosal cell populations

A total of 306,372 esophageal cells (7,856 mean cells per sample) were retained for cell clustering and gene expression analysis (**Figure 1**). Each cell type was identified according to the expression of established cell-specific gene markers including *KRT6A, KRT13,* and *KRT15* for epithelial cells (**Supplemental Table 3**, **Supplemental Figure 1**). Epithelial cells comprised the bulk of the sample (n=264,858; 86.45%), followed by lymphoid cells (n=25,129; 8.20%), myeloid cells (n=10,019; 3.27%), endothelial cells (n=4,027; 1.31%), and all other cell types (n=2,339; 0.76%).

Significant loss of superficial EECs in SSc

Following isolation of the epithelial cell cluster and additional quality control (**Supplemental Figure 2, A-C**), we characterized the remaining 230,720 esophageal epithelial cells (EECs) according to their differentiation and cell cycling states (**Figure 2A**). We classified the EECs into five primary compartments: basal (n=55,818; 24%), proliferating basal (n=36,439; 16%), proliferating suprabasal (n=25,314; 11%), suprabasal (n=82,283; 36%), and superficial (n=30,866; 13%) based on relative expression of canonical epithelial genes and cell cycle markers (**Figure 2, B-C; Supplemental Figure 2, D-E**). Roughly 40% of basal cells and 24% of suprabasal cells were proliferating, and the fractions of cells that were proliferating did not differ by disease (**Figure 2D; Supplemental Figure 2, F-I**). Proportions of basal and suprabasal cells were not significantly different across conditions, but there were significantly fewer superficial cells in SSc compared to HCs (μ_{SSc}=0.10, μ_{HC}=0.21, P=0.003, **Figure 2E**). The reduction of superficial cells in SSc was further apparent when examining EEC differentiation score distributions (**Supplemental Figure 3**) and projecting UMAP embeddings separately by disease state (**Figure 3**).

EEC gene dysregulation highly correlated in SSc and GERD, limited to superficial cells

Overall, the gene expression correlation between biopsy locations was extremely high, ranging from r=0.98 to r=0.99 for the 2,000 most variable genes (**Supplemental Figure 4A**) aggregated by condition and epithelial compartment (**Supplemental Figure 4B**; **Supplemental Table 4**). Inter-sample expression correlations indicated that the greatest gene expression heterogeneity was in the superficial compartment (mean=0.94, std. dev.=0.027), followed by the basal compartment (mean=0.94, std. dev.=0.018; **Figure 4, A-B**). Differential gene expression between conditions was most predominant in the superficial compartment (**Figure 4, C-E**). At the single-cell level, about 6.6% and 4.1% of expressed genes were significantly differentially expressed between SSc and HCs in the superficial compartment in the proximal and distal regions, respectively, compared to just 1.3-1.4% and 1.3-3.0% in non-proliferating basal and suprabasal cells (**Supplemental Tables 5-6**). Most differentially expressed genes (DEGs) were only differentially expressed in one epithelial compartment (**Figure 4, C-D**). We observed more suprabasal differential expression in the distal esophagus than in the proximal esophagus for both SSc and GERD

(**Figure 4, C-E**). Many of the same genes were significantly dysregulated in both SSc and GERD compared to HCs (**Supplemental Table 5**). Depending on the compartment and biopsy location, 22-44% of significantly dysregulated genes in SSc or GERD were differentially expressed in both conditions (**Figure 4E**). Consequently, the DEGs in SSc and GERD were significantly enriched for some of the same pathways, particularly those related to the extracellular matrix and keratinization (**Figure 4F**). Clustered trajectories of relative gene expression (SSc vs. HCs) by epithelial differentiation score for all single-cell-level DEGs revealed distinct patterns of differential expression (**Figure 4, G-H**), which were principally distinguished by the direction of gene expression change in superficial cells. Gene expression changes were more pronounced in the most terminally differentiated superficial cells in the proximal esophagus (**Figure 4G**), whereas in the distal esophagus the differences appeared more in late-stage suprabasal and early-stage superficial cells (**Figure 4H**).

Six pathways were significantly enriched among DEGs between SSc and HCs: matrisome (suprabasal, distal $P_{FDR}=2.3\times10^{-4}$, **Figure 4H**; superficial, distal $P_{FDR}=2.6\times10^{-2}$) and matrisome-associated genes (suprabasal, distal $P_{FDR}=4.4\times10^{-4}$); cornified envelope formation (suprabasal, distal $P_{FDR}=2.1\times10^{-3}$; superficial, distal $P_{FDR}=4.7\times10^{-2}$), and keratinization genes (suprabasal, distal $P_{FDR}=2.1\times10^{-3}$; superficial, distal $P_{FDR}=5.0\times10^{-2}$); developmental biology-related genes (suprabasal, distal $P_{FDR}=4.1\times10^{-4}$; superficial, distal $P_{FDR}=9.2\times10^{-3}$); and innate immune system genes ($P_{FDR}=2.8\times10^{-2}$, **Figure 4G**). No pathways were significantly enriched among genes differentially expressed between SSc and GERD in any epithelial compartment. The leading edges of significantly enriched pathways (**Supplemental Table 7**) contained recurring genes from shared protein families, including serine protease inhibitors (serpins, **Supplemental Figure 4C**), keratins (**Supplemental Figure 4D**), S100 proteins (**Supplemental Figure 4E**), and small proline-rich proteins (SPRRs, **Supplemental Figure 4F**). The most frequent gene in leading edges of significantly enriched pathways was *PI3* (**Supplemental Figure 4G**), including all pathways enriched in SSc. Among the other most enriched pathways specific to SSc were those related to the regulation of metal and immune homeostasis (**Figure 4F**, **Supplemental Table 7**).

Upon aggregating single-cell expression counts by sample for each EEC compartment, we found that gene expression patterns clustered by EEC compartment (**Supplemental Figure 5A**) and that differential expression between conditions was nearly exclusively limited to superficial cells (**Figure 5, A-B; Supplemental Figure 5B**). There were 3,572 genes differentially expressed between SSc and HCs with FDR q<0.05 in the superficial compartment, compared to just 232 total in all other compartments, including only 172 that were not also differentially expressed in the superficial compartment (**Supplemental Table 8**). The differential expression observed in SSc was again highly correlated with the changes seen in GERD (**Figure 5, C-D**). The correlations in $\log_2$ fold change between SSc and GERD vs. HCs were consistently between 0.40-0.53 in all compartments except for superficial cells, where we observed much stronger correlation in the proximal region (r=0.82) than in the distal region (r=0.36; **Supplemental Figure 5C**).

We detected 2,103 genes that were significantly differentially expressed in SSc but not GERD in the proximal esophagus and 282 in the distal esophagus, of which 170 were differentially expressed only in the distal region (**Figure 5, C-D**; **Supplemental Table 9**). Among the most upregulated SSc-specific genes (**Figure 5, C-E; Supplemental Figure 5, C-D**) were genes related to inflammation (*PTGES*, *MFGE8*)[67,68], innate immune response (*FCGBP, BST2*, *CD44*, *APOBEC3A*)[69-72], immune cell migration (*C10orf99*, *LTB4R*, *ACKR3*)[73-75], antigen presentation (*HLA-B*, *CD74*, *TAP1*, *PSMB8*, *PSMB9*)[76], natural killer cell activation (*CLEC2B*)[77], and fibroproliferation (*SGK1*, *HBEGF*)[78,79]. Four of the top five and eight of the top 20 most downregulated SSc-specific genes by fold change in superficial EECs in the proximal esophagus were metallothioneins (*MT1A*, *MT1E*, *MT1F*, *MT1G*, *MT1H*, *MT1M*, *MT1X*, *MT2A*). The metallothioneins comprised the bulk of three pathways uniquely enriched in SSc with P<0.001: zinc homeostasis, copper homeostasis, and cellular responses to stimuli (**Figure 4F**). The most down-regulated SSc-specific gene across both the proximal and distal esophagus was the *H19* lncRNA. Interestingly, the most down-regulated gene by fold change in GERD, *MUC22*, was not differentially expressed in SSc. One gene, *SLC8A1-AS1*, was significantly differentially expressed in both GERD and SSc, but in opposite directions (**Figure 5, C-E; Supplemental Table 9**).

More genes were significantly differentially expressed in SSc than in GERD, but in terms of relative fold change vs. HCs, we observed greater expression changes in GERD (**Supplemental Figure 5C**). We therefore performed all possible sample permutations with equal numbers of SSc and GERD samples (n=4) and repeated differential gene expression testing to more directly compare the relative number of DEGs in both conditions (**Figure 5F**). In superficial cells from the proximal esophagus, there were more DEGs in SSc in 60% of permutations, but the relative FC differences were greater in GERD in 61% of permutations (**Supplemental Table 10**). In the distal region, there were more DEGs in GERD in 62% of permutations, and the relative FC differences were greater in GERD in all permutations. The correlations between SSc and GERD in terms of relative gene expression changes were consistently much higher in the proximal region permutations than in the distal region (**Figure 5, G-H**). The permutation results confirmed that the differences in gene expression observed in SSc relative to GERD were not simply due to differences in sample size.

In summary, the gene expression changes measured in SSc and GERD were highly correlated. In the distal esophagus, differential expression was more pronounced in GERD than in SSc, whereas in the proximal esophagus there were more DEGs in SSc. In both conditions, differential gene expression was most prevalent in the superficial compartment, but the expression changes appeared comparatively earlier in the differentiation of distal EECs relative to proximal EECs.

Transcription factor enrichment analysis

We next examined whether DEGs in SSc superficial cells were significantly enriched for targets of specific transcription factors. Among genes differentially expressed in SSc compared to GERD, the target genes of IRF1 were significantly enriched (**Table 2**). IRF1 targets were significantly enriched among all proximal superficial DEGs (p_{adj}=0.021) and among only those that were downregulated (p_{adj}=0.0024). However, *IRF1* was not itself differentially expressed in superficial cells in SSc compared to GERD. Compared to HCs, three transcription factors were significantly enriched in SSc in the proximal esophagus, including MYC ($p_{adj}=2.1\times10^{-7}$) and E2F4 ($p_{adj}=5.5\times10^{-5}$) for upregulated DEGs and NFE2L2 for downregulated

DEGs ($p_{adj}=7.6\times10^{-4}$). *MYC* and *E2F4* were also themselves differentially expressed in SSc compared to HCs in superficial cells ($p_{adj}=7.8\times10^{-5}$, $p_{adj}=9.8\times10^{-4}$, respectively). MYC was the most enriched transcription factor in genes upregulated in GERD compared to HCs, but the enrichment was not significant after adjusting for multiple testing ($p_{adj}=0.11$). No transcription factors were significantly enriched in any pairwise comparison in the distal esophagus.

Expression mapping in superficial EECs

Examining the expression patterns within superficial cells from the proximal esophagus more closely, we identified five distinct clusters (**Figure 6A**) distinguished by unique expression marker patterns (**Figure 6B, Supplemental Figure 6, Supplemental Table 11**) and varying degrees of differentiation **(Figure 6C)**. Clusters 1 and 3 represent the outermost, terminally differentiated epithelial layers, as evidenced by their *FLG* expression[80-82]. They differed by the expression of metallothioneins, which were predominantly expressed in cluster 3 (**Figure 6, E-F**). Cluster 3 was less abundant in SSc compared to HC with $P<0.05$ (**Figure 6D**), but metallothionein expression was lower in other superficial clusters, as well (**Figure 6F**). Within the superficial EECs, the relative expression of metallothioneins was significantly correlated with the differentiation score ($r=0.06$, $P=2.3\times10^{-23}$). Cluster 2 was distinguished by its relatively high *CTSV* expression. Clusters 4 and 5 were the least differentiated of the superficial cells and were distinguished by their relative expression of *GJB6* and *FGFBP1*, respectively, although neither gene was differentially expressed between conditions.

For the expression of the significantly enriched transcription factors (IRF1, MYC, E2F4, and NFE2L2; **Table 2**) and their targets, we observed two consistent patterns (**Figure 7**). First, the greatest magnitude differences in median target expression between SSc and HCs were seen in cluster 5. Second, in each of those instances, the median target expression in GERD was between that of SSc and HCs. The expression correlations between the enriched transcription factors and their targets were positive for *MYC* ($r=0.42$) and *E2F4* ($r=0.24$) and negative for *IRF1* ($r=-0.20$) and *NFE2L2* ($r=-0.18$).

401

402 ***FLI1* not expressed in human EECs**

403 Deletion of the *Fli1* gene in epithelial cells in mice has been shown to recapitulate histological and
404 molecular features of esophageal involvement in SSc[24]. Therefore, we investigated the expression of *FLI1*
405 in our human esophageal samples. The expression of *FLI1* in human EECs was negligible and did not meet
406 the minimum expression thresholds for inclusion in our differential gene expression analysis. We did
407 observe low *FLI1* expression levels in endothelial cells (**Supplemental Figure 7A**), but the expression
408 differences between SSc, HCs, and GERD was not significant (**Supplemental Figure 7B**). There were
409 many FLI1 downstream targets among the proximal, superficial DEGs between SSc and HCs and seven
410 between SSc and GERD (*ARPC2*, *RAB24*, *MTPN*, *PPIF* upregulated; *CEBPZ*, *TRMT10C*, *TBP*
411 downregulated); however, the proportion of these genes among all DEGs was not different than what would
412 be expected by chance (P>0.05), and the average expression of FLI1 targets was higher in GERD and lower
413 in HCs compared to the expression in SSc (**Supplemental Figure 7C**).

414

415 **Correlations with clinical phenotypes**

416 We next evaluated whether the cellular and molecular changes we observed between SSc, GERD, and HCs
417 were correlated with specific clinical measures of esophageal dysfunction (**Table 1**). To test for associations
418 with esophageal motility phenotypes, we performed ordinal regression against increasing phenotype
419 severity. To more efficiently model the covariance structure among quantitative, functional esophageal
420 measures in SSc (**Figure 8A**), we performed PCA on a set of nine clinical metrics and tested for correlations
421 with the first two PCs (**Figure 8B**). The first PC explained 45.5% of variance and was most correlated with
422 FLIP intra-balloon pressure at 60ml (r=0.94), The second PC explained 22.6% of variance and was most
423 correlated with HRM basal EGJ pressure (r=0.74).

424 We did not observe any significant correlations between epithelial cell compartment proportions in
425 SSc and esophageal motility phenotypes. It appeared that the low proportion of superficial cells in the
426 esophageal epithelium was a universal feature in SSc, regardless of phenotype (**Supplemental Figure 8A**).

The proportion of superficial cells decreased with disease duration, but the trend was not statistically significant (P=0.1; **Supplemental Figure 8B**). We also did not observe any significant correlations between EEC compartment proportions and quantitative trait PCs (**Figure 8C**).

We then tested for correlations with gene expression in superficial EECs for genes that were significantly differentially expressed in SSc compared to HCs ($P_{adj}<0.05$) and nominally differentially expressed in SSc compared to GERD ($P<0.05$). There were 433 genes that met these criteria in the proximal esophagus and 99 in the distal esophagus. Although no associations with esophageal motility phenotypes were statistically significant after adjusting for multiple testing, the strongest phenotypic correlation was with *TRIM11* ($P_{FLIP}=0.01$, $P_{HRM}=0.007$, **Supplemental Figure 8C**), a gene recently found to attenuate Treg cell differentiation in $CD4^+$ T cells in mice[83]. No associations with the top two clinical PCs were significant after adjusting for multiple testing. We also tested for clinical PC correlations with aggregate metallothionein gene expression and transcription factor target expression for IRF1, MYC, E2F4, and NFE2L2. We observed one nominal association between the mean metallothionein module score and PC1 (P=0.02, **Figure 8D**). Notably, within superficial cells we also observed a strong correlation between the proportion of metallothionein-expressing cluster 3 cells and PC1 in the distal esophagus (**Figure 8E**). This indicates that not only is this population of cells reduced in SSc, but its relative decrease is further correlated with more severe esophageal involvement (**Figure 8F**). Therefore, our findings suggest that increased esophageal dysmotility in SSc is associated with a decline in metallothionein-expressing superficial EECs, which coincides with lower overall metallothionein expression in superficial cells.

DISCUSSION

Esophageal dysfunction is extremely common in SSc and is significantly associated with increased mortality and lower quality of life[84,85]. The causal mechanisms by which SSc affects the esophagus, however, have not been conclusively determined. Here, we sought to clarify the role of epithelial cells in SSc esophageal dysfunction by using scRNA-seq to quantify cellular and transcriptional changes relative

453 to HCs and individuals with GERD. While our findings indicate that epithelial changes in SSc result
454 primarily from chronic acid exposure, they also highlight immunoregulatory pathways uniquely altered in
455 SSc that may be linked to pathogenic aberrations.

456 With epithelial layers of the skin and internal organs being primary sites of injury in SSc, the
457 pathogenic role of epithelial cells in SSc has long been an ongoing area of research. When damaged,
458 epithelial cells release signals that help induce fibroblast activation to promote wound healing[86]. In SSc,
459 epidermal keratinocyte characteristics resemble a pro-fibrotic, activated state[87]. SSc epidermal cells were
460 also found to stimulate fibroblasts in culture[88], and some signs related to epithelial-mesenchymal transition
461 (EMT) have been observed in the SSc epidermis[89]. The FLI1 (friend leukemia integration 1) transcription
462 factor, in particular, has received much attention for its potential role in epithelial-cell-mediated SSc
463 pathogenesis[20]. Lower FLI1 expression was observed in the epidermis of diffuse cutaneous SSc, and
464 inactivation of FLI1 in human keratinocytes in vitro induced gene expression changes characteristic of
465 SSc[24]. Furthermore, conditional deletion of *Fli1* in epithelial cells produced an SSc-like phenotype in
466 mice[24]. Importantly, the epithelial-cell-specific *Fli1* knockout further recapitulated the esophageal
467 involvement of SSc, with increased collagen deposition in the lamina propria combined with atrophy of the
468 circular muscle layer, and the esophageal changes were not mediated by T-cell autoimmunity[24]. In contrast
469 to these previous studies in mice and epidermal keratinocytes, we did not observe *FLI1* expression in EECs
470 in any condition. *FLI1* was expressed at low levels in endothelial cells, but the expression differences
471 between SSc, HCs, and GERD were not significant. We did observe significantly increased expression in
472 SSc and GERD of the *PI3* gene, which encodes trappin-2/elafin, previously found to be induced by Fli1
473 silencing in human dermal microvascular endothelial cells[90]. However, this association is unlikely to be
474 pathogenic, as the increase in gene expression was greater in GERD, and a growing body of evidence
475 indicates that trappin-2/elafin is expressed to promote tissue repair in response to gastrointestinal tissue
476 inflammation[91].

477 While there have been many studies of epithelial cells in skin in SSc, molecular study of the human
478 esophagus in SSc had heretofore been limited to one array-based gene expression study in bulk tissue

479 conducted by Taroni and colleagues[15], in which they identified distinct expression signatures among
480 variable genes between 15 individuals with SSc that were similar to those seen in skin[92]. These signatures
481 were independent of clinically defined SSc subsets[15], suggestive of inter-individual heterogeneity in SSc.
482 They also found that gene expression patterns between upper and lower esophageal biopsies within
483 individuals were nearly identical. They did not observe statistical associations between inflammatory gene
484 expression signatures and GERD, but the study was underpowered for such an analysis, and GERD was
485 defined based on histological evidence for basal cell hyperplasia and intraepithelial lymphocyte counts.

486 The gene expression differences we observed in SSc epithelial cells were highly correlated with
487 those seen in GERD, and nearly all differential gene expression was limited to the superficial layers of the
488 epithelium. These observations suggest that the primary driver of differential gene expression in EECs in
489 SSc is chronic acid exposure. The genes with the strongest mutual upregulation in SSc and GERD were
490 primarily related to keratinization/cornification, including small proline-rich proteins (SPRRs), serine
491 protease inhibitors (serpins), S100 proteins, late cornified envelope (LCE) genes, and keratins associated
492 with terminal epithelial differentiation, namely *KRTDAP* and *KRT*. *KRT1* helps maintain epithelial barrier
493 function in gastrointestinal epithelial cells, and its overexpression was shown to attenuate IL-1β-induced
494 epithelial permeability[93]. The mutual upregulation of these genes in the outer layers of the epithelium
495 therefore likely represent a protective response to chronic acid exposure.

496 While the overall gene expression differences were highly correlated between SSc and GERD,
497 there were sets of genes disproportionately upregulated in SSc that hint at disease-related immune response
498 aberrations, including genes that have previously been implicated in SSc pathogenesis. For example,
499 *PTGES*, which encodes prostaglandin E synthase, was previously found to be significantly upregulated in
500 SSc fibroblasts[94] and inflammatory non-classical monocytes[95], and Ptges-null mice were resistant to
501 bleomycin-induced fibrosis[94]. CD44 and CD74 form the receptor complex for the macrophage inhibitory
502 factor (MIF), an inflammatory cytokine that promotes fibroblast migration and has been implicated in SSc
503 pathogenesis[96]. LTB4R (Leukotriene B4 Receptor, or BLT1) has been found to activate AKT/mTOR
504 signaling and knockdown of *LTB4R* attenuated fibrosis in bleomycin-induced SSc in murine models[97].

Serum HBEGF (heparin-binding epidermal growth factor) levels and fibroblast *HBEGF* expression were both significantly elevated in SSc[98]. Copy number variation of *APOBEC3A* was significantly associated with SSc in a Han Chinese population[99]. Finally, the SSc-specific upregulation of genes involved in antigen processing and presentation (*HLA-B*, *CD74*, *TAP1*, *PSMB8*, *PSMB9*) are suggestive of increased human leukocyte antigen (HLA) class I activity in superficial EECs in SSc. Notably, *TAP1*, *PSMB8*, and *PSMB9* are located immediately adjacent to one another in the class II region of the HLA locus, which is the genomic region with the strongest genetic associations with SSc[100], and SSc-associated HLA-B alleles have also been identified[101,102].

The most striking set of genes that were uniquely downregulated in SSc were metallothioneins. The expression of detected metallothioneins (*MT1A*, *MT1E*, *MT1F*, *MT1G*, *MT1H*, *MT1M*, *MT1X*, *MT2A*) was strongly induced in the superficial compartment of EECs, but significantly less so in SSc and, interestingly, only in the proximal esophagus. We further observed a nominal association between relative metallothionein expression in the proximal esophagus and the first PC of esophageal dysmotility among SSc patients, with lower expression of metallothioneins correlated with greater EGJ distensibility and weaker contractility. The proportion of the primary metallothionein-expressing cluster within superficial EECs was likewise significantly associated with clinical PC1. The metallothioneins are a family of well-conserved, metal-binding proteins that regulate zinc and copper homeostasis, prevent heavy metal poisoning, and combat oxidative stress[103,104]. Their study in a wide array of physiological conditions and immune-mediated diseases has revealed the proteins play central roles in innate and adaptive immunity, including autoimmunity, but their immunoregulatory behavior is highly complex and context-specific[103,104]. Given their import in immune regulation, their associations with SSc and esophageal motility reported in this study, and the connection between SSc and heavy metal exposure[105], the metallothioneins are compelling candidates that warrant further study in SSc.

Interestingly, there was greater relative gene dysregulation in the proximal esophagus compared to the distal esophagus in SSc, but the opposite was true for GERD. This discrepancy suggests that esophageal dysmotility in SSc leads to greater acid exposure in the proximal esophagus, since refluxed gastric acid

typically affects the distal esophagus significantly more than the proximal esophagus[106] and abnormal peristalsis prolongs acid clearance[107]. This finding coincides with a bulk RNA-seq study of esophageal mucosa of achalasia patients[108], which likewise identified more differential expression in the proximal esophagus than in the distal esophagus, including significant enrichment of matrisome-associated genes and lower expression of genes associated with reactive oxygen species metabolism[108]. Due to differences in innervation depth[109], the epithelium of the proximal esophagus has more nociceptive sensitivity than the distal esophagus, which likely contributes to the association between gastrointestinal symptoms and lower quality of life in SSc[110]. Proximal acid exposure increases the risk of aspiration[111] and is significantly more prevalent in SSc patients with idiopathic lung fibrosis[112].

Targets for several transcription factors, including IRF1, MYC, E2F4, and NFE2L2 (or NRF2), were significantly enriched among DEGs in superficial EECs from the proximal esophagus. IRF1 is involved innate immune responses, but while IRF1 targets were enriched in DEGs between SSc and GERD, the enrichment appeared to be driven by upregulation in GERD. IRF1 targets were not enriched in DEGs between SSc and HCs, nor was *IRF1* significantly differentially expressed in SSc. MYC, E2F4, and NFE2L2 all participate in different stages of the cell cycle[113-115], and expression of each was highest in either the proliferating basal or suprabasal compartments, but these proteins may also play a role in terminal differentiation of EECs, particularly under conditions of stress. In the least differentiated superficial cluster (cluster 5), where the expression differences relative to HCs for each of these transcription factors and their targets was most pronounced, the expression level changes in GERD were correlated with those observed in SSc. Furthermore, Myc ablation in Krt14-expressing tissues in mice led to abnormal terminal differentiation of epithelial cells[116], and a study of the esophageal epithelium in Nrf2 knockout mice indicated that Nrf2 regulates cornification of keratinized epithelial cells under conditions of stress[117].

There are important limitations to consider when interpreting this study. First, this study only focused on squamous epithelial cells. There may be relevant changes in other cell types within the esophageal mucosa that correlate with SSc and dysmotility, but such analyses are ongoing and were outside the scope of this investigation. Second, the relatively small patient sample size of this study combined with

the heterogeneity of SSc subtypes and dysmotility phenotypes limited our power to detect clinical associations between cell type proportions or gene expression changes and specific clinical phenotypes. Heterogeneous molecular profiles in SSc esophagus samples have been described previously[15], but we grouped all SSc patients together in our analyses for comparisons against GERD and HCs. We applied ordinal logistic regression on motility classifications and performed principal components analysis on reflux- and motility-related quantitative traits to increase our power to detect clinical associations but were nonetheless statistically limited by sample size. Third, we did not examine imaging data in the SSc esophageal mucosa. Therefore, we cannot make conclusions on the morphological states that accompany the transcriptional and cellular proportion changes that we observed. Future studies utilizing larger, more homogeneous cohorts with imaging data may be able to detect more esophageal epithelial changes associated with dysmotility in SSc.

In summary, esophageal complications are common in individuals with SSc and can greatly impact quality of life and lifespan. In this study, we sought to clarify the role of the epithelium in SSc esophageal involvement. Through a thorough, single-cell-level transcriptomic investigation, we identified the unique cellular and transcriptional differences present in the SSc esophageal epithelium. There were significantly fewer terminally differentiated epithelial cells in the outermost, superficial layers in both the proximal and distal esophagus, but otherwise epithelial compartment proportions were similar to healthy controls, including proliferating cell proportions. Significant differences in gene expression were likewise almost exclusively found in the superficial compartment, and these changes were highly correlated with those seen in individuals with GERD, indicating that the primary driver of differential gene expression in the SSc esophageal epithelium is chronic acid exposure. Transcriptional differences were also more prominent in the proximal esophagus of SSc patients, suggesting that esophageal dysmotility leads to greater proximal exposure. Genes that were most disproportionately dysregulated in SSc compared to GERD belonged to immune-related pathways, including innate and adaptive response, antigen presentation, and metal homeostasis, and may therefore point to pathogenic immune dysfunction. Future studies investigating these pathways in non-epithelial cell populations in more homogeneous SSc cohorts may further resolve the

583 pathogenic mechanisms driving esophageal involvement in SSc. By serving as an atlas for the human
584 esophageal epithelium in SSc, this study can guide future efforts to address remaining gaps in our
585 understanding of the SSc esophagus, to ultimately uncover pathogenic mechanisms and identify actionable
586 targets.

REFERENCES

1. Bairkdar, M., Rossides, M., Westerlind, H., Hesselstrand, R., Arkema, E.V., and Holmqvist, M. (2021). Incidence and prevalence of systemic sclerosis globally: a comprehensive systematic review and meta-analysis. Rheumatology (Oxford) *60*, 3121-3133. 10.1093/rheumatology/keab190.
2. Fan, Y., Bender, S., Shi, W., and Zoz, D. (2020). Incidence and prevalence of systemic sclerosis and systemic sclerosis with interstitial lung disease in the United States. J Manag Care Spec Pharm *26*, 1539-1547. 10.18553/jmcp.2020.20136.
3. Tian, J., Kang, S., Zhang, D., Huang, Y., Zhao, M., Gui, X., Yao, X., and Lu, Q. (2023). Global, regional, and national incidence and prevalence of systemic sclerosis. Clin Immunol *248*, 109267. 10.1016/j.clim.2023.109267.
4. Pope, J.E., Quansah, K., Hassan, S., Seung, S.J., Flavin, J., and Kolb, M. (2021). Systemic Sclerosis and Associated Interstitial Lung Disease in Ontario, Canada: An Examination of Prevalence and Survival Over 10 Years. J Rheumatol *48*, 1427-1434. 10.3899/jrheum.201049.
5. Li, J.X. (2022). Secular Trends in Systemic Sclerosis Mortality in the United States from 1981 to 2020. Int J Environ Res Public Health *19*. 10.3390/ijerph192215088.
6. Rubio-Rivas, M., Royo, C., Simeon, C.P., Corbella, X., and Fonollosa, V. (2014). Mortality and survival in systemic sclerosis: systematic review and meta-analysis. Semin Arthritis Rheum *44*, 208-219. 10.1016/j.semarthrit.2014.05.010.
7. Bairkdar, M., Chen, E.Y., Dickman, P.W., Hesselstrand, R., Westerlind, H., and Holmqvist, M. (2023). Survival in Swedish patients with systemic sclerosis: a nationwide population-based matched cohort study. Rheumatology (Oxford) *62*, 1170-1178. 10.1093/rheumatology/keac474.
8. Li, B., Yan, J., Pu, J., Tang, J., Xu, S., and Wang, X. (2021). Esophageal Dysfunction in Systemic Sclerosis: An Update. Rheumatol Ther *8*, 1535-1549. 10.1007/s40744-021-00382-0.
9. Emmanuel, A. (2016). Current management of the gastrointestinal complications of systemic sclerosis. Nat Rev Gastroenterol Hepatol *13*, 461-472. 10.1038/nrgastro.2016.99.
10. Ahuja, N.K., and Clarke, J.O. (2021). Scleroderma and the Esophagus. Gastroenterol Clin North Am *50*, 905-918. 10.1016/j.gtc.2021.08.005.
11. Denaxas, K., Ladas, S.D., and Karamanolis, G.P. (2018). Evaluation and management of esophageal manifestations in systemic sclerosis. Ann Gastroenterol *31*, 165-170. 10.20524/aog.2018.0228.
12. Foocharoen, C., Thinkhamrop, W., Chaichaya, N., Mahakkanukrauh, A., Suwannaroj, S., and Thinkhamrop, B. (2022). Development and validation of machine learning for early mortality in systemic sclerosis. Sci Rep *12*, 17178. 10.1038/s41598-022-22161-9.
13. Sjogren, R.W. (1994). Gastrointestinal motility disorders in scleroderma. Arthritis Rheum *37*, 1265-1282. 10.1002/art.1780370902.
14. Roberts, C.G., Hummers, L.K., Ravich, W.J., Wigley, F.M., and Hutchins, G.M. (2006). A case-control study of the pathology of oesophageal disease in systemic sclerosis (scleroderma). Gut *55*, 1697-1703. 10.1136/gut.2005.086074.
15. Taroni, J.N., Martyanov, V., Huang, C.C., Mahoney, J.M., Hirano, I., Shetuni, B., Yang, G.Y., Brenner, D., Jung, B., Wood, T.A., et al. (2015). Molecular characterization of systemic sclerosis esophageal pathology identifies inflammatory and proliferative signatures. Arthritis Res Ther *17*, 194. 10.1186/s13075-015-0695-1.
16. Roman, S., Hot, A., Fabien, N., Cordier, J.F., Miossec, P., Ninet, J., Mion, F., and Reseau Sclerodermie des Hospices Civils de, L. (2011). Esophageal dysmotility associated with systemic sclerosis: a high-resolution manometry study. Dis Esophagus *24*, 299-304. 10.1111/j.1442-2050.2010.01150.x.
17. Noviani, M., Chellamuthu, V.R., Albani, S., and Low, A.H.L. (2022). Toward Molecular Stratification and Precision Medicine in Systemic Sclerosis. Front Med (Lausanne) *9*, 911977. 10.3389/fmed.2022.911977.

18. Carlson, D.A., Crowell, M.D., Kimmel, J.N., Patel, A., Gyawali, C.P., Hinchcliff, M., Griffing, W.L., Pandolfino, J.E., and Vela, M.F. (2016). Loss of Peristaltic Reserve, Determined by Multiple Rapid Swallows, Is the Most Frequent Esophageal Motility Abnormality in Patients With Systemic Sclerosis. Clin Gastroenterol Hepatol *14*, 1502-1506. 10.1016/j.cgh.2016.03.039.
19. Kimmel, J.N., Carlson, D.A., Hinchcliff, M., Carns, M.A., Aren, K.A., Lee, J., and Pandolfino, J.E. (2016). The association between systemic sclerosis disease manifestations and esophageal high-resolution manometry parameters. Neurogastroenterol Motil *28*, 1157-1165. 10.1111/nmo.12813.
20. Asano, Y., Takahashi, T., and Saigusa, R. (2019). Systemic sclerosis: Is the epithelium a missing piece of the pathogenic puzzle? J Dermatol Sci *94*, 259-265. 10.1016/j.jdermsci.2019.04.007.
21. Durcan, C., Hossain, M., Chagnon, G., Peric, D., Karam, G., Bsiesy, L., and Girard, E. (2022). Experimental investigations of the human oesophagus: anisotropic properties of the embalmed mucosa-submucosa layer under large deformation. Biomech Model Mechanobiol *21*, 1685-1702. 10.1007/s10237-022-01613-1.
22. Kou, W., Pandolfino, J.E., Kahrilas, P.J., and Patankar, N.A. (2017). Simulation studies of the role of esophageal mucosa in bolus transport. Biomech Model Mechanobiol *16*, 1001-1009. 10.1007/s10237-016-0867-1.
23. Asano, Y., Bujor, A.M., and Trojanowska, M. (2010). The impact of Fli1 deficiency on the pathogenesis of systemic sclerosis. J Dermatol Sci *59*, 153-162. 10.1016/j.jdermsci.2010.06.008.
24. Takahashi, T., Asano, Y., Sugawara, K., Yamashita, T., Nakamura, K., Saigusa, R., Ichimura, Y., Toyama, T., Taniguchi, T., Akamata, K., et al. (2017). Epithelial Fli1 deficiency drives systemic autoimmunity and fibrosis: Possible roles in scleroderma. J Exp Med *214*, 1129-1151. 10.1084/jem.20160247.
25. Dinh, H.Q., Pan, F., Wang, G., Huang, Q.F., Olingy, C.E., Wu, Z.Y., Wang, S.H., Xu, X., Xu, X.E., He, J.Z., et al. (2021). Integrated single-cell transcriptome analysis reveals heterogeneity of esophageal squamous cell carcinoma microenvironment. Nat Commun *12*, 7335. 10.1038/s41467-021-27599-5.
26. Zhang, X., Peng, L., Luo, Y., Zhang, S., Pu, Y., Chen, Y., Guo, W., Yao, J., Shao, M., Fan, W., et al. (2021). Dissecting esophageal squamous-cell carcinoma ecosystem by single-cell transcriptomic analysis. Nat Commun *12*, 5291. 10.1038/s41467-021-25539-x.
27. Rochman, M., Wen, T., Kotliar, M., Dexheimer, P.J., Ben-Baruch Morgenstern, N., Caldwell, J.M., Lim, H.W., and Rothenberg, M.E. (2022). Single-cell RNA-Seq of human esophageal epithelium in homeostasis and allergic inflammation. JCI Insight *7*. 10.1172/jci.insight.159093.
28. Clevenger, M.H., Karami, A.L., Carlson, D.A., Kahrilas, P.J., Gonsalves, N., Pandolfino, J.E., Winter, D.R., Whelan, K.A., and Tetreault, M.P. (2023). Suprabasal cells retain progenitor cell identity programs in eosinophilic esophagitis-driven basal cell hyperplasia. JCI Insight *8*. 10.1172/jci.insight.171765.
29. Carlson, D.A., Prescott, J.E., Germond, E., Brenner, D., Carns, M., Correia, C.S., Tetreault, M.P., McMahan, Z.H., Hinchcliff, M., Kou, W., et al. (2022). Heterogeneity of primary and secondary peristalsis in systemic sclerosis: A new model of "scleroderma esophagus". Neurogastroenterol Motil *34*, e14284. 10.1111/nmo.14284.
30. Carlson, D.A., Gyawali, C.P., Khan, A., Yadlapati, R., Chen, J., Chokshi, R.V., Clarke, J.O., Garza, J.M., Jain, A.S., Katz, P., et al. (2021). Classifying Esophageal Motility by FLIP Panometry: A Study of 722 Subjects With Manometry. Am J Gastroenterol *116*, 2357-2366. 10.14309/ajg.0000000000001532.
31. Koop, A.H., Kahrilas, P.J., Schauer, J., Pandolfino, J.E., and Carlson, D.A. (2023). The impact of primary peristalsis, contractile reserve, and secondary peristalsis on esophageal clearance measured by timed barium esophagogram. Neurogastroenterol Motil, e14638. 10.1111/nmo.14638.
32. Yadlapati, R., Kahrilas, P.J., Fox, M.R., Bredenoord, A.J., Prakash Gyawali, C., Roman, S., Babaei, A., Mittal, R.K., Rommel, N., Savarino, E., et al. (2021). Esophageal motility disorders on high-resolution manometry: Chicago classification version 4.0((c)). Neurogastroenterol Motil *33*, e14058. 10.1111/nmo.14058.

33. Stern, E.K., Carlson, D.A., Falmagne, S., Hoffmann, A.D., Carns, M., Pandolfino, J.E., Hinchcliff, M., and Brenner, D.M. (2018). Abnormal esophageal acid exposure on high-dose proton pump inhibitor therapy is common in systemic sclerosis patients. Neurogastroenterol Motil *30*. 10.1111/nmo.13247.
34. Yadlapati, R., Kahrilas, P.J., Fox, M.R., Bredenoord, A.J., Prakash Gyawali, C., Roman, S., Babaei, A., Mittal, R.K., Rommel, N., Savarino, E., et al. (2021). Esophageal motility disorders on high-resolution manometry: Chicago classification version 4.0(©). Neurogastroenterol Motil *33*, e14058. 10.1111/nmo.14058.
35. Rooney, K.P., Baumann, A.J., Donnan, E., Kou, W., Triggs, J.R., Prescott, J., Decorrevont, A., Dorian, E., Kahrilas, P.J., Pandolfino, J.E., and Carlson, D.A. (2021). Esophagogastric Junction Opening Parameters Are Consistently Abnormal in Untreated Achalasia. Clin Gastroenterol Hepatol *19*, 1058-1060.e1051. 10.1016/j.cgh.2020.03.069.
36. Carlson, D.A., Baumann, A.J., Donnan, E.N., Krause, A., Kou, W., and Pandolfino, J.E. (2021). Evaluating esophageal motility beyond primary peristalsis: Assessing esophagogastric junction opening mechanics and secondary peristalsis in patients with normal manometry. Neurogastroenterol Motil *33*, e14116. 10.1111/nmo.14116.
37. Carlson, D.A., Kou, W., Lin, Z., Hinchcliff, M., Thakrar, A., Falmagne, S., Prescott, J., Dorian, E., Kahrilas, P.J., and Pandolfino, J.E. (2019). Normal Values of Esophageal Distensibility and Distension-Induced Contractility Measured by Functional Luminal Imaging Probe Panometry. Clin Gastroenterol Hepatol *17*, 674-681 e671. 10.1016/j.cgh.2018.07.042.
38. Jonasson, C., Wernersson, B., Hoff, D.A., and Hatlebakk, J.G. (2013). Validation of the GerdQ questionnaire for the diagnosis of gastro-oesophageal reflux disease. Aliment Pharmacol Ther *37*, 564-572. 10.1111/apt.12204.
39. Taft, T.H., Riehl, M., Sodikoff, J.B., Kahrilas, P.J., Keefer, L., Doerfler, B., and Pandolfino, J.E. (2016). Development and validation of the brief esophageal dysphagia questionnaire. Neurogastroenterol Motil *28*, 1854-1860. 10.1111/nmo.12889.
40. Bedell, A., Taft, T.H., Keefer, L., and Pandolfino, J. (2016). Development of the Northwestern Esophageal Quality of Life Scale: A Hybrid Measure for Use Across Esophageal Conditions. Am J Gastroenterol *111*, 493-499. 10.1038/ajg.2016.20.
41. Hao, Y., Hao, S., Andersen-Nissen, E., Mauck, W.M., 3rd, Zheng, S., Butler, A., Lee, M.J., Wilk, A.J., Darby, C., Zager, M., et al. (2021). Integrated analysis of multimodal single-cell data. Cell *184*, 3573-3587 e3529. 10.1016/j.cell.2021.04.048.
42. Hippen, A.A., Falco, M.M., Weber, L.M., Erkan, E.P., Zhang, K., Doherty, J.A., Vaharautio, A., Greene, C.S., and Hicks, S.C. (2021). miQC: An adaptive probabilistic framework for quality control of single-cell RNA-sequencing data. PLoS Comput Biol *17*, e1009290. 10.1371/journal.pcbi.1009290.
43. Germain, P.L., Lun, A., Garcia Meixide, C., Macnair, W., and Robinson, M.D. (2021). Doublet identification in single-cell sequencing data using scDblFinder. F1000Res *10*, 979. 10.12688/f1000research.73600.2.
44. Hafemeister, C., and Satija, R. (2019). Normalization and variance stabilization of single-cell RNA-seq data using regularized negative binomial regression. Genome Biol *20*, 296. 10.1186/s13059-019-1874-1.
45. Lause, J., Berens, P., and Kobak, D. (2021). Analytic Pearson residuals for normalization of single-cell RNA-seq UMI data. Genome Biol *22*, 258. 10.1186/s13059-021-02451-7.
46. McInnes, L., Healy, J., and Melville, J. (2018). UMAP: Uniform Manifold Approximation and Projection for Dimension Reduction. arXiv:1802.03426. 10.48550/arXiv.1802.03426.
47. Clevenger, M.H., Karami, A.L., Carlson, D.A., Kahrilas, P.J., Gonsalves, N., Pandolfino, J.E., Winter, D.R., Whelan, K.A., and Tetreault, M.P. (2023). Suprabasal cells retaining stem cell identity programs drive basal cell hyperplasia in eosinophilic esophagitis. bioRxiv. 10.1101/2023.04.20.537495.

48. Busslinger, G.A., Weusten, B.L.A., Bogte, A., Begthel, H., Brosens, L.A.A., and Clevers, H. (2021). Human gastrointestinal epithelia of the esophagus, stomach, and duodenum resolved at single-cell resolution. Cell Rep *34*, 108819. 10.1016/j.celrep.2021.108819.
49. Kabir, M.F., Karami, A.L., Cruz-Acuna, R., Klochkova, A., Saxena, R., Mu, A., Murray, M.G., Cruz, J., Fuller, A.D., Clevenger, M.H., et al. (2022). Single cell transcriptomic analysis reveals cellular diversity of murine esophageal epithelium. Nat Commun *13*, 2167. 10.1038/s41467-022-29747-x.
50. Okumura, T., Shimada, Y., Imamura, M., and Yasumoto, S. (2003). Neurotrophin receptor p75(NTR) characterizes human esophageal keratinocyte stem cells in vitro. Oncogene *22*, 4017-4026. 10.1038/sj.onc.1206525.
51. Tirosh, I., Izar, B., Prakadan, S.M., Wadsworth, M.H., 2nd, Treacy, D., Trombetta, J.J., Rotem, A., Rodman, C., Lian, C., Murphy, G., et al. (2016). Dissecting the multicellular ecosystem of metastatic melanoma by single-cell RNA-seq. Science *352*, 189-196. 10.1126/science.aad0501.
52. Fonseka, C.Y., Rao, D.A., Teslovich, N.C., Korsunsky, I., Hannes, S.K., Slowikowski, K., Gurish, M.F., Donlin, L.T., Lederer, J.A., Weinblatt, M.E., et al. (2018). Mixed-effects association of single cells identifies an expanded effector CD4(+) T cell subset in rheumatoid arthritis. Sci Transl Med *10*. 10.1126/scitranslmed.aaq0305.
53. Mootha, V.K., Lindgren, C.M., Eriksson, K.F., Subramanian, A., Sihag, S., Lehar, J., Puigserver, P., Carlsson, E., Ridderstrale, M., Laurila, E., et al. (2003). PGC-1alpha-responsive genes involved in oxidative phosphorylation are coordinately downregulated in human diabetes. Nat Genet *34*, 267-273. 10.1038/ng1180.
54. Subramanian, A., Tamayo, P., Mootha, V.K., Mukherjee, S., Ebert, B.L., Gillette, M.A., Paulovich, A., Pomeroy, S.L., Golub, T.R., Lander, E.S., and Mesirov, J.P. (2005). Gene set enrichment analysis: a knowledge-based approach for interpreting genome-wide expression profiles. Proc Natl Acad Sci U S A *102*, 15545-15550. 10.1073/pnas.0506580102.
55. Liberzon, A., Birger, C., Thorvaldsdottir, H., Ghandi, M., Mesirov, J.P., and Tamayo, P. (2015). The Molecular Signatures Database (MSigDB) hallmark gene set collection. Cell Syst *1*, 417-425. 10.1016/j.cels.2015.12.004.
56. Squair, J.W., Gautier, M., Kathe, C., Anderson, M.A., James, N.D., Hutson, T.H., Hudelle, R., Qaiser, T., Matson, K.J.E., Barraud, Q., et al. (2021). Confronting false discoveries in single-cell differential expression. Nat Commun *12*, 5692. 10.1038/s41467-021-25960-2.
57. Chen, Y., Lun, A.T., and Smyth, G.K. (2016). From reads to genes to pathways: differential expression analysis of RNA-Seq experiments using Rsubread and the edgeR quasi-likelihood pipeline. F1000Res *5*, 1438. 10.12688/f1000research.8987.2.
58. McCarthy, D.J., Chen, Y., and Smyth, G.K. (2012). Differential expression analysis of multifactor RNA-Seq experiments with respect to biological variation. Nucleic Acids Res *40*, 4288-4297. 10.1093/nar/gks042.
59. Robinson, M.D., McCarthy, D.J., and Smyth, G.K. (2010). edgeR: a Bioconductor package for differential expression analysis of digital gene expression data. Bioinformatics *26*, 139-140. 10.1093/bioinformatics/btp616.
60. Wu, T., Hu, E., Xu, S., Chen, M., Guo, P., Dai, Z., Feng, T., Zhou, L., Tang, W., Zhan, L., et al. (2021). clusterProfiler 4.0: A universal enrichment tool for interpreting omics data. Innovation (Camb) *2*, 100141. 10.1016/j.xinn.2021.100141.
61. Consortium, E.P. (2012). An integrated encyclopedia of DNA elements in the human genome. Nature *489*, 57-74. 10.1038/nature11247.
62. Lachmann, A., Xu, H., Krishnan, J., Berger, S.I., Mazloom, A.R., and Ma'ayan, A. (2010). ChEA: transcription factor regulation inferred from integrating genome-wide ChIP-X experiments. Bioinformatics *26*, 2438-2444. 10.1093/bioinformatics/btq466.
63. Kou, Y., Chen, E.Y., Clark, N.R., Duan, Q., Tan, C.M., and Ma'ayan, A. (2013). ChEA2: Gene-Set Libraries from ChIP-X Experiments to Decode the Transcription Regulome. held in Berlin, Heidelberg, (Springer Berlin Heidelberg), pp. 416-430.

64. Chen, E.Y., Tan, C.M., Kou, Y., Duan, Q., Wang, Z., Meirelles, G.V., Clark, N.R., and Ma'ayan, A. (2013). Enrichr: interactive and collaborative HTML5 gene list enrichment analysis tool. BMC Bioinformatics *14*, 128. 10.1186/1471-2105-14-128.
65. Hou, W., Ji, Z., Chen, Z., Wherry, E.J., Hicks, S.C., and Ji, H. (2023). A statistical framework for differential pseudotime analysis with multiple single-cell RNA-seq samples. Nat Commun *14*, 7286. 10.1038/s41467-023-42841-y.
66. Koop, A.H., Kahrilas, P.J., Schauer, J., Pandolfino, J.E., and Carlson, D.A. (2023). The impact of primary peristalsis, contractile reserve, and secondary peristalsis on esophageal clearance measured by timed barium esophagogram. Neurogastroenterol Motil *35*, e14638. 10.1111/nmo.14638.
67. Wang, Q., Li, Y., Wu, M., Huang, S., Zhang, A., Zhang, Y., and Jia, Z. (2021). Targeting microsomal prostaglandin E synthase 1 to develop drugs treating the inflammatory diseases. Am J Transl Res *13*, 391-419.
68. Yi, Y.S. (2016). Functional Role of Milk Fat Globule-Epidermal Growth Factor VIII in Macrophage-Mediated Inflammatory Responses and Inflammatory/Autoimmune Diseases. Mediators Inflamm *2016*, 5628486. 10.1155/2016/5628486.
69. Oh, S., Bournique, E., Bowen, D., Jalili, P., Sanchez, A., Ward, I., Dananberg, A., Manjunath, L., Tran, G.P., Semler, B.L., et al. (2021). Genotoxic stress and viral infection induce transient expression of APOBEC3A and pro-inflammatory genes through two distinct pathways. Nat Commun *12*, 4917. 10.1038/s41467-021-25203-4.
70. Tiwari, R., de la Torre, J.C., McGavern, D.B., and Nayak, D. (2019). Beyond Tethering the Viral Particles: Immunomodulatory Functions of Tetherin (BST-2). DNA Cell Biol *38*, 1170-1177. 10.1089/dna.2019.4777.
71. Baaten, B.J., Li, C.R., and Bradley, L.M. (2010). Multifaceted regulation of T cells by CD44. Commun Integr Biol *3*, 508-512. 10.4161/cib.3.6.13495.
72. Liu, Q., Niu, X., Li, Y., Zhang, J.R., Zhu, S.J., Yang, Q.Y., Zhang, W., and Gong, L. (2022). Role of the mucin-like glycoprotein FCGBP in mucosal immunity and cancer. Front Immunol *13*, 863317. 10.3389/fimmu.2022.863317.
73. Okamoto, Y., and Shikano, S. (2023). Emerging roles of a chemoattractant receptor GPR15 and ligands in pathophysiology. Front Immunol *14*, 1179456. 10.3389/fimmu.2023.1179456.
74. Subramanian, B.C., Moissoglu, K., and Parent, C.A. (2018). The LTB(4)-BLT1 axis regulates the polarized trafficking of chemoattractant GPCRs during neutrophil chemotaxis. J Cell Sci *131*. 10.1242/jcs.217422.
75. Nguyen, H.T., Reyes-Alcaraz, A., Yong, H.J., Nguyen, L.P., Park, H.K., Inoue, A., Lee, C.S., Seong, J.Y., and Hwang, J.I. (2020). CXCR7: a beta-arrestin-biased receptor that potentiates cell migration and recruits beta-arrestin2 exclusively through Gbetagamma subunits and GRK2. Cell Biosci *10*, 134. 10.1186/s13578-020-00497-x.
76. Kelly, A., and Trowsdale, J. (2019). Genetics of antigen processing and presentation. Immunogenetics *71*, 161-170. 10.1007/s00251-018-1082-2.
77. Bartel, Y., Bauer, B., and Steinle, A. (2013). Modulation of NK cell function by genetically coupled C-type lectin-like receptor/ligand pairs encoded in the human natural killer gene complex. Front Immunol *4*, 362. 10.3389/fimmu.2013.00362.
78. Lu, R.Q., Zhang, Y.Y., Zhao, H.Q., Guo, R.Q., Jiang, Z.X., and Guo, R. (2022). SGK1, a Critical Regulator of Immune Modulation and Fibrosis and a Potential Therapeutic Target in Chronic Graft-Versus-Host Disease. Front Immunol *13*, 822303. 10.3389/fimmu.2022.822303.
79. Li, Y., Su, G., Zhong, Y., Xiong, Z., Huang, T., Quan, J., Huang, J., Wen, X., Luo, C., Zheng, W., et al. (2021). HB-EGF-induced IL-8 secretion from airway epithelium leads to lung fibroblast proliferation and migration. BMC Pulm Med *21*, 347. 10.1186/s12890-021-01726-w.
80. Uhlen, M., Fagerberg, L., Hallstrom, B.M., Lindskog, C., Oksvold, P., Mardinoglu, A., Sivertsson, A., Kampf, C., Sjostedt, E., Asplund, A., et al. (2015). Proteomics. Tissue-based map of the human proteome. Science *347*, 1260419. 10.1126/science.1260419.

81. Politi, E., Angelakopoulou, A., Grapsa, D., Zande, M., Stefanaki, K., Panagiotou, I., Roma, E., and Syrigou, E. (2017). Filaggrin and Periostin Expression Is Altered in Eosinophilic Esophagitis and Normalized With Treatment. J Pediatr Gastroenterol Nutr *65*, 47-52. 10.1097/MPG.0000000000001419.
82. Oshima, N., Ishihara, S., Fukuba, N., Mishima, Y., Kawashima, K., Ishimura, N., Ishikawa, N., Maruyama, R., and Kinoshita, Y. (2017). Epidermal differentiation complex protein involucrin is down-regulated in eosinophilic esophagitis. Esophagus *14*, 171-177. 10.1007/s10388-016-0568-y.
83. Yu, T., Yang, X., Fu, Q., Liang, J., Wu, X., Sheng, J., Chen, Y., Xiao, L., Wu, Y., Nie, D., et al. (2023). TRIM11 attenuates Treg cell differentiation by p62-selective autophagic degradation of AIM2. Cell Rep *42*, 113231. 10.1016/j.celrep.2023.113231.
84. Crowell, M.D., Umar, S.B., Griffing, W.L., DiBaise, J.K., Lacy, B.E., and Vela, M.F. (2017). Esophageal Motor Abnormalities in Patients With Scleroderma: Heterogeneity, Risk Factors, and Effects on Quality of Life. Clin Gastroenterol Hepatol *15*, 207-213 e201. 10.1016/j.cgh.2016.08.034.
85. Forbes, A., and Marie, I. (2009). Gastrointestinal complications: the most frequent internal complications of systemic sclerosis. Rheumatology (Oxford) *48 Suppl 3*, iii36-39. 10.1093/rheumatology/ken485.
86. Krieg, T., Abraham, D., and Lafyatis, R. (2007). Fibrosis in connective tissue disease: the role of the myofibroblast and fibroblast-epithelial cell interactions. Arthritis Res Ther *9 Suppl 2*, S4. 10.1186/ar2188.
87. Aden, N., Shiwen, X., Aden, D., Black, C., Nuttall, A., Denton, C.P., Leask, A., Abraham, D., and Stratton, R. (2008). Proteomic analysis of scleroderma lesional skin reveals activated wound healing phenotype of epidermal cell layer. Rheumatology (Oxford) *47*, 1754-1760. 10.1093/rheumatology/ken370.
88. Aden, N., Nuttall, A., Shiwen, X., de Winter, P., Leask, A., Black, C.M., Denton, C.P., Abraham, D.J., and Stratton, R.J. (2010). Epithelial cells promote fibroblast activation via IL-1alpha in systemic sclerosis. J Invest Dermatol *130*, 2191-2200. 10.1038/jid.2010.120.
89. Nikitorowicz-Buniak, J., Denton, C.P., Abraham, D., and Stratton, R. (2015). Partially Evoked Epithelial-Mesenchymal Transition (EMT) Is Associated with Increased TGFbeta Signaling within Lesional Scleroderma Skin. PLoS One *10*, e0134092. 10.1371/journal.pone.0134092.
90. Miyagawa, T., Asano, Y., Saigusa, R., Hirabayashi, M., Yamashita, T., Taniguchi, T., Takahashi, T., Nakamura, K., Miura, S., Yoshizaki, A., et al. (2019). A potential contribution of trappin-2 to the development of vasculopathy in systemic sclerosis. J Eur Acad Dermatol Venereol *33*, 753-760. 10.1111/jdv.15387.
91. Deraison, C., Bonnart, C., Langella, P., Roget, K., and Vergnolle, N. (2023). Elafin and its precursor trappin-2: What is their therapeutic potential for intestinal diseases? Br J Pharmacol *180*, 144-160. 10.1111/bph.15985.
92. Hinchcliff, M., Huang, C.C., Wood, T.A., Matthew Mahoney, J., Martyanov, V., Bhattacharyya, S., Tamaki, Z., Lee, J., Carns, M., Podlusky, S., et al. (2013). Molecular signatures in skin associated with clinical improvement during mycophenolate treatment in systemic sclerosis. J Invest Dermatol *133*, 1979-1989. 10.1038/jid.2013.130.
93. Dong, X., Liu, Z., Lan, D., Niu, J., Miao, J., Yang, G., Zhang, F., Sun, Y., Wang, K., and Miao, Y. (2017). Critical role of Keratin 1 in maintaining epithelial barrier and correlation of its down-regulation with the progression of inflammatory bowel disease. Gene *608*, 13-19. 10.1016/j.gene.2017.01.015.
94. McCann, M.R., Monemdjou, R., Ghassemi-Kakroodi, P., Fahmi, H., Perez, G., Liu, S., Shi-Wen, X., Parapuram, S.K., Kojima, F., Denton, C.P., et al. (2011). mPGES-1 null mice are resistant to bleomycin-induced skin fibrosis. Arthritis Res Ther *13*, R6. 10.1186/ar3226.
95. Villanueva-Martin, G., Acosta-Herrera, M., Carmona, E.G., Kerick, M., Ortego-Centeno, N., Callejas-Rubio, J.L., Mages, N., Klages, S., Borno, S., Timmermann, B., et al. (2023). Non-classical circulating monocytes expressing high levels of microsomal prostaglandin E2 synthase-1

tag an aberrant IFN-response in systemic sclerosis. J Autoimmun *140*, 103097. 10.1016/j.jaut.2023.103097.

96. Unlu, B., Tursen, U., Rajabi, Z., Jabalameli, N., and Rajabi, F. (2022). The Immunogenetics of Systemic Sclerosis. Adv Exp Med Biol *1367*, 259-298. 10.1007/978-3-030-92616-8_10.
97. Liang, M., Lv, J., Jiang, Z., He, H., Chen, C., Xiong, Y., Zhu, X., Xue, Y., Yu, Y., Yang, S., et al. (2020). Promotion of Myofibroblast Differentiation and Tissue Fibrosis by the Leukotriene B(4) - Leukotriene B(4) Receptor Axis in Systemic Sclerosis. Arthritis Rheumatol *72*, 1013-1025. 10.1002/art.41192.
98. Hirabayashi, M., Asano, Y., Yamashita, T., Miura, S., Nakamura, K., Taniguchi, T., Saigusa, R., Takahashi, T., Ichimura, Y., Miyagawa, T., et al. (2018). Possible pro-inflammatory role of heparin-binding epidermal growth factor-like growth factor in the active phase of systemic sclerosis. J Dermatol *45*, 182-188. 10.1111/1346-8138.14088.
99. Guo, S., Li, Y., Wang, Y., Chu, H., Chen, Y., Liu, Q., Guo, G., Tu, W., Wu, W., Zou, H., et al. (2016). Copy Number Variation of HLA-DQA1 and APOBEC3A/3B Contribute to the Susceptibility of Systemic Sclerosis in the Chinese Han Population. J Rheumatol *43*, 880-886. 10.3899/jrheum.150945.
100. Lopez-Isac, E., Acosta-Herrera, M., Kerick, M., Assassi, S., Satpathy, A.T., Granja, J., Mumbach, M.R., Beretta, L., Simeon, C.P., Carreira, P., et al. (2019). GWAS for systemic sclerosis identifies multiple risk loci and highlights fibrotic and vasculopathy pathways. Nat Commun *10*, 4955. 10.1038/s41467-019-12760-y.
101. Acosta-Herrera, M., Kerick, M., Lopez-Isac, E., Assassi, S., Beretta, L., Simeon-Aznar, C.P., Ortego-Centeno, N., International, S.G., Proudman, S.M., Australian Scleroderma Interest, G., et al. (2021). Comprehensive analysis of the major histocompatibility complex in systemic sclerosis identifies differential HLA associations by clinical and serological subtypes. Ann Rheum Dis *80*, 1040-1047. 10.1136/annrheumdis-2021-219884.
102. Hanson, A.L., Sahhar, J., Ngian, G.S., Roddy, J., Walker, J., Stevens, W., Nikpour, M., Assassi, S., Proudman, S., Mayes, M.D., et al. (2022). Contribution of HLA and KIR Alleles to Systemic Sclerosis Susceptibility and Immunological and Clinical Disease Subtypes. Front Genet *13*, 913196. 10.3389/fgene.2022.913196.
103. Dai, H., Wang, L., Li, L., Huang, Z., and Ye, L. (2021). Metallothionein 1: A New Spotlight on Inflammatory Diseases. Front Immunol *12*, 739918. 10.3389/fimmu.2021.739918.
104. Subramanian Vignesh, K., and Deepe, G.S., Jr. (2017). Metallothioneins: Emerging Modulators in Immunity and Infection. Int J Mol Sci *18*. 10.3390/ijms18102197.
105. Marie, I. (2019). Systemic sclerosis and exposure to heavy metals. Autoimmun Rev *18*, 62-72. 10.1016/j.autrev.2018.11.001.
106. Shaker, R., Dodds, W.J., Helm, J.F., Kern, M.K., and Hogan, W.J. (1991). Regional esophageal distribution and clearance of refluxed gastric acid. Gastroenterology *101*, 355-359. 10.1016/0016-5085(91)90011-9.
107. Diener, U., Patti, M.G., Molena, D., Fisichella, P.M., and Way, L.W. (2001). Esophageal dysmotility and gastroesophageal reflux disease. J Gastrointest Surg *5*, 260-265. 10.1016/s1091-255x(01)80046-9.
108. Patel, C.K., Kahrilas, P.J., Hodge, N.B., Tsikretsis, L.E., Carlson, D.A., Pandolfino, J.E., and Tetreault, M.P. (2022). RNA-sequencing reveals molecular and regional differences in the esophageal mucosa of achalasia patients. Sci Rep *12*, 20616. 10.1038/s41598-022-25103-7.
109. Woodland, P., Aktar, R., Mthunzi, E., Lee, C., Peiris, M., Preston, S.L., Blackshaw, L.A., and Sifrim, D. (2015). Distinct afferent innervation patterns within the human proximal and distal esophageal mucosa. Am J Physiol Gastrointest Liver Physiol *308*, G525-531. 10.1152/ajpgi.00175.2014.
110. Sandqvist, G., and Hesselstrand, R. (2019). Validity of the Swedish version of the systemic sclerosis quality of life questionnaire (SSCQoL): A novel measure of quality of life for patients with systemic sclerosis. Ann Rheum Dis *78*, 855-857. 10.1136/annrheumdis-2018-214260.

111. Lee, A.S., Lee, J.S., He, Z., and Ryu, J.H. (2020). Reflux-Aspiration in Chronic Lung Disease. Ann Am Thorac Soc *17*, 155-164. 10.1513/AnnalsATS.201906-427CME.
112. Savarino, E., Bazzica, M., Zentilin, P., Pohl, D., Parodi, A., Cittadini, G., Negrini, S., Indiveri, F., Tutuian, R., Savarino, V., and Ghio, M. (2009). Gastroesophageal reflux and pulmonary fibrosis in scleroderma: a study using pH-impedance monitoring. Am J Respir Crit Care Med *179*, 408-413. 10.1164/rccm.200808-1359OC.
113. Conboy, C.M., Spyrou, C., Thorne, N.P., Wade, E.J., Barbosa-Morais, N.L., Wilson, M.D., Bhattacharjee, A., Young, R.A., Tavare, S., Lees, J.A., and Odom, D.T. (2007). Cell cycle genes are the evolutionarily conserved targets of the E2F4 transcription factor. PLoS One *2*, e1061. 10.1371/journal.pone.0001061.
114. Garcia-Gutierrez, L., Delgado, M.D., and Leon, J. (2019). MYC Oncogene Contributions to Release of Cell Cycle Brakes. Genes (Basel) *10*. 10.3390/genes10030244.
115. Lastra, D., Escoll, M., and Cuadrado, A. (2022). Transcription Factor NRF2 Participates in Cell Cycle Progression at the Level of G1/S and Mitotic Checkpoints. Antioxidants (Basel) *11*. 10.3390/antiox11050946.
116. Portal, C., Wang, Z., Scott, D.K., Wolosin, J.M., and Iomini, C. (2022). The c-Myc Oncogene Maintains Corneal Epithelial Architecture at Homeostasis, Modulates p63 Expression, and Enhances Proliferation During Tissue Repair. Invest Ophthalmol Vis Sci *63*, 3. 10.1167/iovs.63.2.3.
117. Wruck, C.J., Wruck, A., Brandenburg, L.O., Kadyrov, M., Tohidnezhad, M., and Pufe, T. (2011). Impact of Nrf2 on esophagus epithelium cornification. Int J Dermatol *50*, 1362-1365. 10.1111/j.1365-4632.2011.04989.x.
118. Jones, R., Junghard, O., Dent, J., Vakil, N., Halling, K., Wernersson, B., and Lind, T. (2009). Development of the GerdQ, a tool for the diagnosis and management of gastro-oesophageal reflux disease in primary care. Aliment Pharmacol Ther *30*, 1030-1038. 10.1111/j.1365-2036.2009.04142.x.

966 **FIGURES**

967 **Figure 1. ScRNA-seq sample composition by cell type. A)** Integrated UMAP embedding of all cells
968 (n=306,372) labeled by cell type. **B)** Expression by cell type of canonical markers. **C)** Sample-wise (n=39)
969 distribution of major cell types. **D)** Proportion of cells by cell type.

970

971 **Figure 2. Landscape of esophageal epithelial cells. A)** Histological summary of the human esophageal
972 epithelium, adopted from Clevenger et al.[28] Alternatively shaded cells within the same layer represent
973 proliferating cells. NOTE: The layers of replicating cells not attached to the basement membrane, labeled
974 here as proliferating suprabasal cells, are sometimes referred to as epibasal cells[28]. **B)** Integrated UMAP
975 embedding of all esophageal epithelial cells (EECs, n=230,720) labeled by epithelial compartment. **C)**
976 Expression by EEC compartment and cell cycle markers. **C)** Proportion of proliferating basal and
977 suprabasal cells by condition and biopsy location. **E)** Proportions of cells by condition, EEC compartment,
978 and biopsy location. The bars denote the mean values, the vertical lines the standard deviations, and the
979 points the individual sample proportions. Pairwise differences across conditions were evaluated statistically
980 using MASC[52]. *p<0.05; **p<0.005.

981

982 **Figure 3. Distribution of esophageal epithelial cells by differentiation score and epithelial**
983 **compartment. A)** Integrated UMAP embeddings of esophageal epithelial cells divided by disease state,
984 colored by differentiation score. **B)** Swarm plots of esophageal epithelial cells by differentiation score,
985 colored by epithelial compartment.

986

987 **Figure 4. Differential gene expression at single-cell resolution in esophageal epithelial cells. A)** Inter-
988 sample expression correlations are shown for each epithelial compartment for the 2,000 most variable
989 genes. **B)** The distribution of inter-sample expression correlations are shown by epithelial compartment. **C-**
990 **D)** UpSet plots showing differential gene expression at the single-cell level by epithelial compartment for
991 SSc vs HCs (purple) and GERD vs HCs (orange) in the proximal **(C)** and distal **(D)** esophagus. **E)** The
992 number of significantly differentially expressed genes with $|\log_2 FC| > 0.1$ are shown for SSC vs. HCs and
993 GERD vs. HCs, by non-proliferating epithelial compartment and biopsy location. **F)** Gene set enrichment

analysis results, showing all pathways enriched with P<0.001 (unadjusted) for SSc vs. HCs (purple) and GERD vs. HCs (orange), split by non-proliferating epithelial compartment and biopsy location. Pathways in bold had enrichment with P<0.001 in both SSc and GERD. Points circled in red indicate statistical significance after adjusting for the number of tested pathways (P_{FDR}<0.05). **G-H)** Relative gene expression (SSc vs. HCs) for all DEGs at the single-cell level were modeled using Lamian[65] and plotted against the epithelial differentiation score in the proximal **(G)** and distal **(H)** esophagus. These trajectories were clustered based on Euclidean distance using Ward's method. The lefthand color bar displays the blended color of all epithelial compartments in which each gene was differentially expressed. In **G)**, labeled genes highlight the top 25 ranked genes in the leading edge of the innate immune system pathway enriched in SSc in the superficial compartment of the proximal esophagus. In **H)**, the labeled genes mark the leading edge genes of the matrisome pathway enriched in SSc in the suprabasal compartment of the distal esophagus. **I-L)** Dot plots showing average gene expression, by condition and epithelial compartment, for the most highly represented protein families in the leading edges of significantly enriched pathways: keratins **(I)**, S100 proteins **(J)**, small proline-rich proteins **(K)**, and serine protease inhibitors **(L)**. **M)** Single-cell gene expression by condition, epithelial compartment, and esophageal region for *PI3*, the most frequent gene in leading edges of significantly enriched pathways.

Figure 5. Differential gene expression aggregated by sample and EEC compartment. A-B) Gene expression differences between SSc and HCs **(A)** and between SSc and GERD **(B)** are shown for each EEC compartment. Significant DEGs (FDR<0.05) are highlighted in purple. The percentages of genes that were significantly differentially expressed in each compartment are plotted in blue in along the secondary Y axis. **C-D)** Gene expression differences in log_2FC are shown for SSc vs. HCs (Y axis) against GERD vs. HCs (X axis) within the superficial compartment in the proximal **(C)** and distal **(D)** regions. Significant DEGs in both conditions are highlighted in blue, significant DEGs in SSC only are highlighted in purple, and significant DEGs in GERD only are highlighted in orange. The correlation between comparisons is shown in the upper left, and the slope and coefficient of determination for the modeled linear regression with intercept=0 is displayed in the lower right. Trendlines with 95% confidence intervals are plotted in pink, and the dashed grey lines denote where y=x. Encircled points highlight disease-specific DEGs that are

referenced in the main text and plotted in **(E)**, which shows the distribution of expression aggregated by sample in the superficial compartment across conditions and biopsy locations. Pairwise differential expression was determined using edgeR's quasi-likelihood F-tests: *p<0.05; **p<0.05; ***p<0.0005. **F)** The number of significant DEGs are shown for GERD vs. HCs (orange) and for all permutations of n=4 samples for SSc vs. HCs (purple) in superficial cells for both proximal and distal regions. The point within the SSc distribution is the median value. **G-H)** The distributions of relative FC or slope *m* **(G)** and coefficient of determination r^2 **(H)** are shown for all permutations of n=4 SSc samples, determined by modeling a linear regression with intercept=0 for the log_2FC of SSc vs. HCs against the log_2FC of GERD vs. HCs for all expressed genes in the superficial compartment for both proximal and distal regions. DEG, differentially expressed gene; FC, fold change.

Figure 6. Landscape of superficial esophageal epithelial cells. A) Integrated UMAP embedding of all superficial EECs (n=30,866) clustered by unique transcriptional signatures. **B)** Relative expression of cluster-specific gene signatures. **C)** Epithelial differentiation score by superficial cell cluster. **D)** Proportion of superficial cells by condition and cluster from the proximal esophagus. The bars denote the mean values, the vertical lines the standard deviations, and the points the individual sample proportions. Pairwise differences across conditions were evaluated statistically using MASC[52]. *p<0.05; **p<0.005. **E)** Distribution of metallothionein module score in proximal, superficial cells by condition. The metallothionein module score included *MT1A*, *MT1E*, *MT1F*, *MT1G*, *MT1H*, *MT1M*, *MT1X*, and *MT2A*. **F)** Distribution of relative metallothionein expression by cluster and condition in superficial cells from proximal esophagus. All pairwise comparisons were between SSc and GERD were statistically significant, except for cluster 5.

Figure 7. Expression of enriched transcription factors and their targets in superficial EECs in proximal esophagus. The distributions of enriched transcription factor expression and target module scores are shown proximal, superficial cells by condition and superficial cluster for **A)** IRF1, **B)** MYC, **C)** E2F4, and **D)** NE2L2.

Figure 8. Correlations with clinical phenotypes. A) Heatmap of quantitative clinical traits organized using agglomerative, complete hierarchical clustering on Euclidean distances, with pairwise Spearman correlations shown in each cell. **B)** SSc cases are plotted on the first two PCs of the quantitative clinical traits, colored by esophageal motility phenotype. The relative magnitude and direction of trait correlations with the PCs are shown with black arrows. **C)** Correlations between EEC compartments and clinical trait PCs in SSc cases. Linear regression trendlines with 95% confidence intervals are shown for each compartment against PC1 and PC2. **D)** Correlations between aggregate, relative metallothionein expression and clinical trait PCs in superficial cells in the proximal esophagus. Trendlines with 95% confidence intervals are shown with the unadjusted correlation P-value. The metallothionein module score included *MT1A*, *MT1E*, *MT1F*, *MT1G*, *MT1H*, *MT1M*, *MT1X*, and *MT2A*. **E)** Correlations between superficial clusters (SCs) and clinical trait PC1 in SSc cases. Linear regression trendlines with 95% confidence intervals are shown for each SC. The displayed P-values correspond to the highlighted correlations between SC3 and PC1. **F)** Boxplots showing the proportion of SC3 in superficial cells by esophageal motility phenotype in the proximal and distal esophagus, colored by disease state (HCs, grey; GERD, orange; SSc, purple). AET, acid exposure time; BEDQ, brief esophageal dysphagia questionnaire; BMI, body mass index; DCI, distal contractile integral; DI, distensibility index; EGJ, esophagogastric junction; EGJOO, esophagogastric junction outflow obstruction; FLIP, functional luminal imaging probe panometry; HCs, healthy controls; HRM, high-resolution manometry; IEM, ineffective esophageal motility; IQR, inter-quartile range; IRP, integrated relaxation pressure; NEQOL, Northwestern esophageal quality of life; NM, neuromyogenic model. NR, not reported.

SUPPLEMENTAL FIGURES

Supplemental Figure 1. Cell clustering and cell type annotation. A) Cell type module scores for 10 detected cell types, colored by relative gene expression of the listed genes. **B)** Projected UMAP embeddings calculated on the top 40 PCs with n=200 neighbors. Cells are colored by cluster, which are numbered in descending order by total cell count. Clusters were determined using Seurat's modularity-based clustering on a shared nearest neighbor (SNN) graph with k=25 and resolution=0.25 on the top 40 PCs. **C)** Isolation of cluster 13 for annotation of cell types with smaller proportions of cells and projected UMAP embeddings for cluster 13, colored by subcluster. **D)** Cell type module scores for 7 detected cell types in subcluster 13, colored by relative gene expression of the listed genes.

Supplemental Figure 2. Epithelial cell quality control and annotation. A) Projected UMAP embeddings for integrated, esophageal epithelial cells (EECs) calculated on the top 35 PCs with n=100 neighbors. Cells are colored by cluster, which are numbered in descending order by total cell count. Clusters were determined using Seurat's modularity-based clustering on a shared nearest neighbor (SNN) graph with k=40 and resolution=0.50 on the top 40 PCs**. B)** EEC UMAP projection, colored by the number of unique genes per cell. **C)** Distribution of number of UMIs detected per cell, split by cluster. EECs with <3500 UMIs/cell were removed from further analysis. **D)** EEC UMAPs colored by gene expression (log(counts+1))) for genes included in compartment-specific expression scores. **E)** EEC UMAPs colored by compartment expression scores. **F)** Projected UMAP embeddings for post-quality-control EECs calculated on the top 35 PCs with n=100 neighbors. Cells are colored by cluster, which are numbered in descending order by total cell count. Clusters were determined using Seurat's modularity-based clustering on a SNN graph with k=50 and resolution=0.25 on the top 35 PCs. **G)** Result of K-means clustering to distinguish suprabasal from basal cells, based on expression of corresponding cluster markers (Supplemental Figure 4) in clusters 3, 4, and 5, with K=2. **H)** Result of K-means clustering to distinguish superficial from suprabasal cells, based on expression of corresponding cluster markers (Supplemental Figure 4) in clusters 6, 7, and 8, with K=2. **I)** Predicted classification of cell cycle state in EECs determined using using Seurat's CellCycleScoring() function.

Supplemental Figure 3. Derivation of epithelial cell differentiation score. A) Density plots of esophageal epithelial cell compartment module scores by compartment annotation. **B)** Density plot of epithelial cell differentiation score by annotated compartment. **C)** UMAP of esophageal epithelial cells colored by differentiation score.

Supplemental Figure 4. Group-wise gene expression correlation for variable genes. A) 2,000 most variable genes among single cells across all samples, with top 20 labeled. **B)** Correlations of gene expression aggregated by condition and biopsy location are shown for each epithelial compartment for the 2,000 most variable genes, with proximal samples along the Y axis and distal samples along the X axis.

Supplemental Figure 5. Differential gene expression aggregated by sample and esophageal epithelial cell compartment. A) Multidimensional scaling plots of aggregate gene expression samples colored by sample, epithelial compartment, condition, and biopsy location. **B)** Volcano plots of differential gene expression between SSc and GERD by epithelial compartment and biopsy location with significant associations highlighted in red and outer significantly differentially expressed genes labeled. **C)** Gene expression differences in $\log_2$FC are shown for SSc vs. HCs (Y axis) against GERD vs. HCs (X axis) for each epithelial compartment in the proximal and distal regions. Outer significantly differentially expressed genes are labeled, as well as immune-related genes uniquely differentially expressed in SSc. The Spearman correlations between gene expression differences are shown in the upper right of each plot (*r*), the relative FC or slope (*m)* and coefficient of determination (r^2) are shown in the bottom right of each plot. Trendlines with 95% confidence intervals are plotted in pink, and the dashed grey lines denote where y=x. **D)** Distributions of aggregate gene expression by epithelial layer, biopsy location, and condition are shown for top SSc-specific and GERD-specific differentially expressed genes.

Supplemental Figure 6. Expression of superficial esophageal epithelial cell markers. UMAPs with expression for the top superficial cluster markers are shown along with the epithelial differentiation score for superficial cells.

Supplemental Figure 7. *FLI1* expression in human esophageal mucosa. A) UMAP of integrated mucosal dataset, colored by *FLI1* expression. The distribution of *FLI1* expression by cell type is shown in the upper right. **B)** Distribution of *FLI1* expression by cell type and disease state. Endothelial cells had the highest *FLI1* expression, but the expression differences between diseases was not significant. **C)** Violin plot of the relative expression of FLI1 target genes in superficial cells.

Supplemental Figure 8. Epithelial cell compartment proportions and additional correlations by motility phenotype. A-B) Proportions of esophageal epithelial cell compartments by HRM **(A)** and FLIP **(B)** esophageal dysmotility phenotypes are shown for the proximal and distal esophagus samples. The bars denote the mean values, the vertical lines the standard deviations, and the points the individual sample proportions. **C)** The relationship between the proportion of superficial cells and the SSc disease duration is plotted for proximal and distal samples. Trendlines with 95% confidence intervals are plotted in pink, and correlation P-values are displayed in the upper right corners. **D)** The distribution of normalized gene expression values by esophageal motility phenotype are shown for the *TRIM11* gene for the FLIP, HRM, and NM esophogeal dysmotility classifications. Unadjusted ordinal regression p-values are displayed in the upper left corners. *TRIM11* was the most strongly association gene with the dysmotility phenotypes by p-value. HRM, high-resolution manometry; FLIP, functional luminal imaging probe panometry; IEM, ineffective esophageal motility; EGJOO, esophagogastric junction outflow obstruction; NM, neuromyogenic model.

TABLES

Table 1. Patient demographics and clinical characteristics

	HCs		SSc		GERD	
Demographics	**N = 6**		**N = 10**		**N = 4**	
Sex – female	5 (83.3%)		9 (90%)		3 (75%)	
Race – white	5 (83.3%)		8 (80%)		2 (50%)	
Ethnicity – non-Hispanic	5 (83.3%)		8 (80%)		2 (50%)	
Race/ethnicity – unknown/NR	1 (16.7%)		2 (20%)		2 (50%)	
Traits	**N**	**Median (IQR)**	**N**	**Median (IQR)**	**N**	**Median (IQR)**
Age (yrs)	6	27 (25-29)	10	54 (47-70)	4	42 (30-56)
BMI (kg/m^2)	6	23 (22-25)	10	22 (19-30)	4	24 (23-36)
Esophageal motility						
Mean DCI (mmHg•s•cm)	6	464.2 (386-6-1026.1)	10	57.5 (0.0-206.1)	2	509.6 (367.4-651.7)
Pressure 60ml (mmHg)	6	43.5 (38.3-54.5)	9	31.0 (30.5-40.3)	0	-
EGJ barrier function						
End-expiratory EGJ pressure (mmHg)	6	7 (4-8)	10	6 (3-10)	2	12 (11-12)
EGJ contractile index (mmHg•cm)	6	19.4 (15.2-29.0)	10	21.0 (19.1-27.5)	2	19.0 (10.8-27.1)
Median IRP (mmHg)	6	4 (3-9)	10	6 (4-12)	2	8 (6-9)
EGJ-DI (mm^2/mmHg)	6	6.2 (5.2-8.5)	9	6.3 (4.1-9.2)	-	-
Reflux severity						
AET (%)	6	0.8 (0.5-2.8)	4	8.7 (3.3-14.5)	3	16.8 (13.9-17.3)
GerdQ[118] score	6	0 (0-0)	10	3 (1-4)	3	3 (3-4)
BEDQ[39] score	6	0 (0-0)	8	8 (3-14)	3	1 (1-1)
NEQOL[40] score	6	56 (56-56)	8	31 (23-47)	3	36 (29-46)

AET, acid exposure time; BEDQ, brief esophageal dysphagia questionnaire; BMI, body mass index; DCI, distal contractile integral; DI, distensibility index; EGJ, esophagogastric junction; HCs, healthy controls; IQR, inter-quartile range; IRP, integrated relaxation pressure; NEQOL, Northwestern esophageal quality of life; NR, not reported

1148

Table 2. Pairwise transcription factor enrichment in superficial cells in proximal esophagus

Comparison	TF	Direction	DEG Targets	DEG Targets / DEGs	TF Targets / Background	P_{adj}	TF Expr. LogFC	TF Expr. P_{adj}
SSc vs. **GERD**	IRF1	**+/-**	7	0.11	0.03	2.9×10^{-2}	0.22	9.0×10^{-1}
		-	5	0.19	0.03	8.9×10^{-3}		
SSc vs. **HCs**	MYC	**+**	120	0.10	0.06	2.1×10^{-7}	1.64	7.8×10^{-5}
	E2F4	**+**	116	0.08	0.06	5.5×10^{-5}	0.88	9.8×10^{-4}
	NFE2L2	**-**	108	0.11	0.07	7.6×10^{-4}	0.25	3.2×10^{-1}

DEG, differentially expressed gene; Expr., expression; GERD, gastroesophageal reflux disease ; HCs, healthy controls; LogFC, $\log_2$ (fold change); SSc, systemic sclerosis; TF, transcription factor.

1149

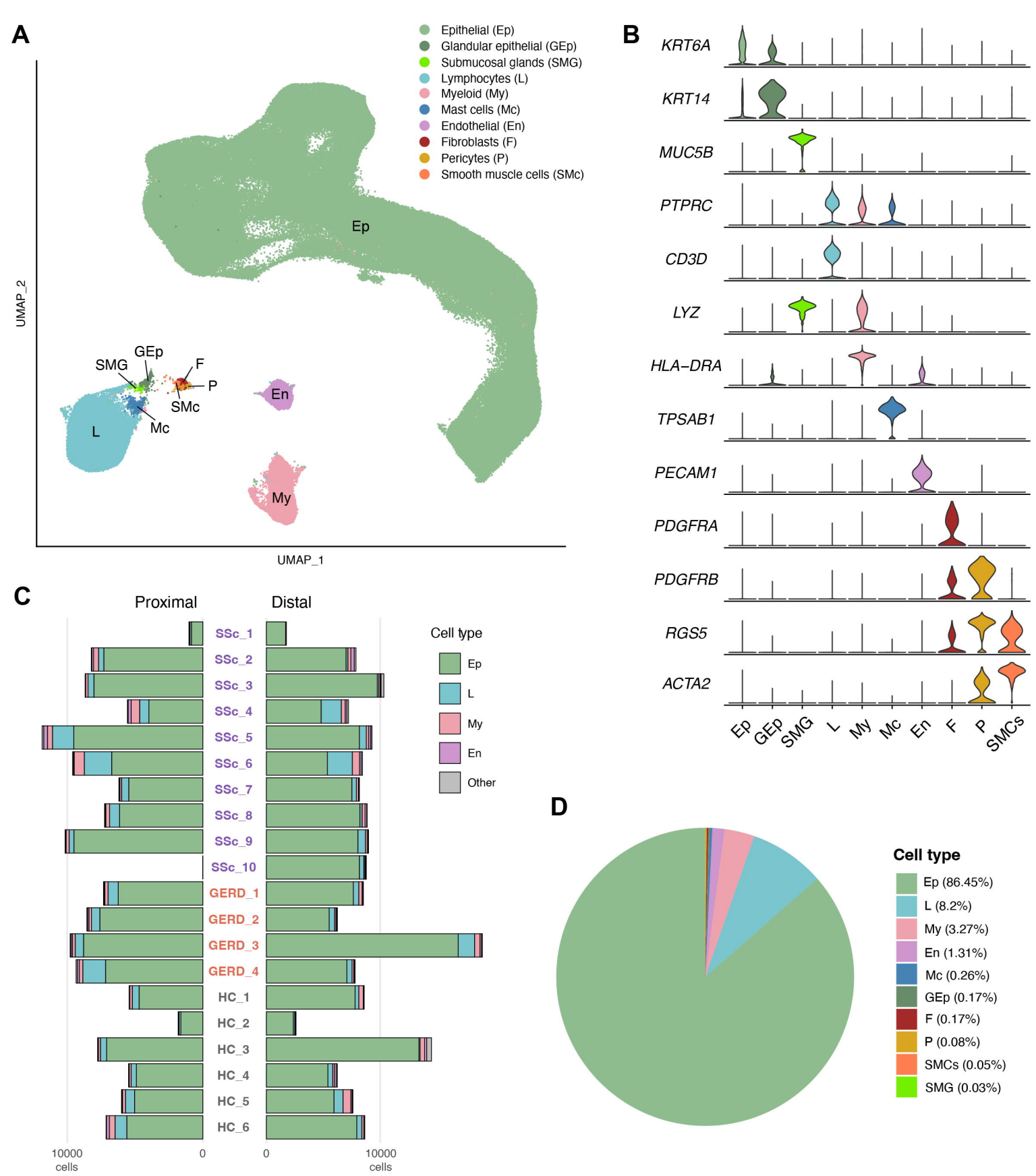
A
Epithelial (Ep)
Glandular epithelial (GEp)
Submucosal glands (SMG)
Lymphocytes (L)
Myeloid (My)
Mast cells (Mc)
Endothelial (En)
Fibroblasts (F)
Pericytes (P)
Smooth muscle cells (SMc)
Ep
SMG
GEp
F
P
SMc
Mc
L
En
My
UMAP_2
UMAP_1
B
KRT6A
KRT14
MUC5B
PTPRC
CD3D
LYZ
HLA−DRA
TPSAB1
PECAM1
PDGFRA
PDGFRB
RGS5
ACTA2
Ep
GEp
SMG
L
My
Mc
En
F
P
SMCs
C
Proximal
Distal
SSc_1
SSc_2
SSc_3
SSc_4
SSc_5
SSc_6
SSc_7
SSc_8
SSc_9
SSc_10
GERD_1
GERD_2
GERD_3
GERD_4
HC_1
HC_2
HC_3
HC_4
HC_5
HC_6
Cell type
Ep
L
My
En
Other
10000
cells
0
0
10000
cells
D
Cell type
Ep (86.45%)
L (8.2%)
My (3.27%)
En (1.31%)
Mc (0.26%)
GEp (0.17%)
F (0.17%)
P (0.08%)
SMCs (0.05%)
SMG (0.03%)

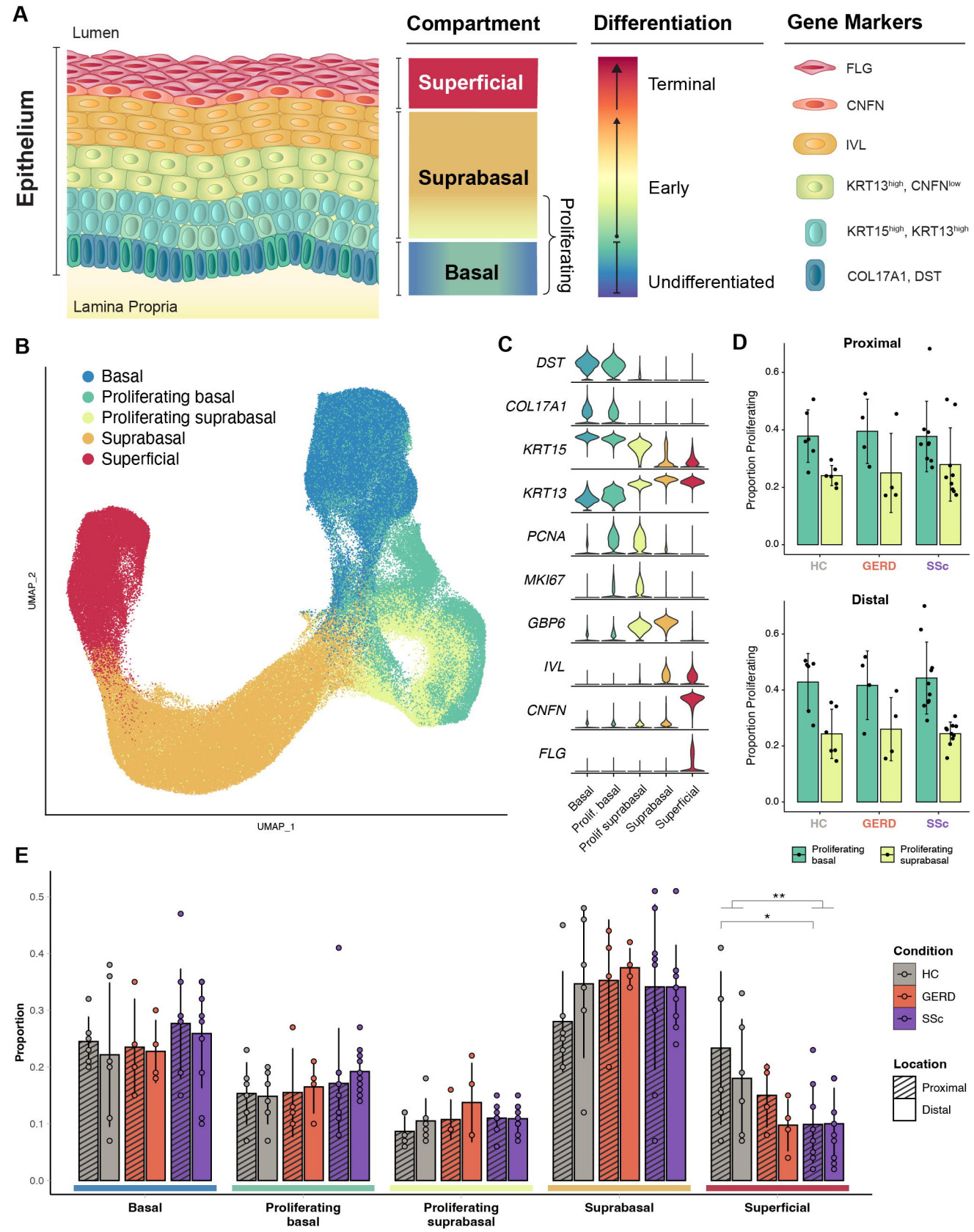
A
Lumen
Epithelium
Lamina Propria
Compartment
Superficial
Suprabasal
Basal
Proliferating
Differentiation
Terminal
Early
Undifferentiated
Gene Markers
FLG
CNFN
IVL
KRT13high, CNFNlow
KRT15high, KRT13high
COL17A1, DST
B
Basal
Proliferating basal
Proliferating suprabasal
Suprabasal
Superficial
UMAP_2
UMAP_1
C
DST
COL17A1
KRT15
KRT13
PCNA
MKI67
GBP6
IVL
CNFN
FLG
Basal
Prolif. basal
Prolif suprabasal
Suprabasal
Superficial
D
Proximal
Distal
Proportion Proliferating
0.0
0.2
0.4
0.6
HC
GERD
SSc
Proliferating basal
Proliferating suprabasal
E
Proportion
0.0
0.1
0.2
0.3
0.4
0.5
**
*
Basal
Proliferating basal
Proliferating suprabasal
Suprabasal
Superficial
Condition
HC
GERD
SSc
Location
Proximal
Distal

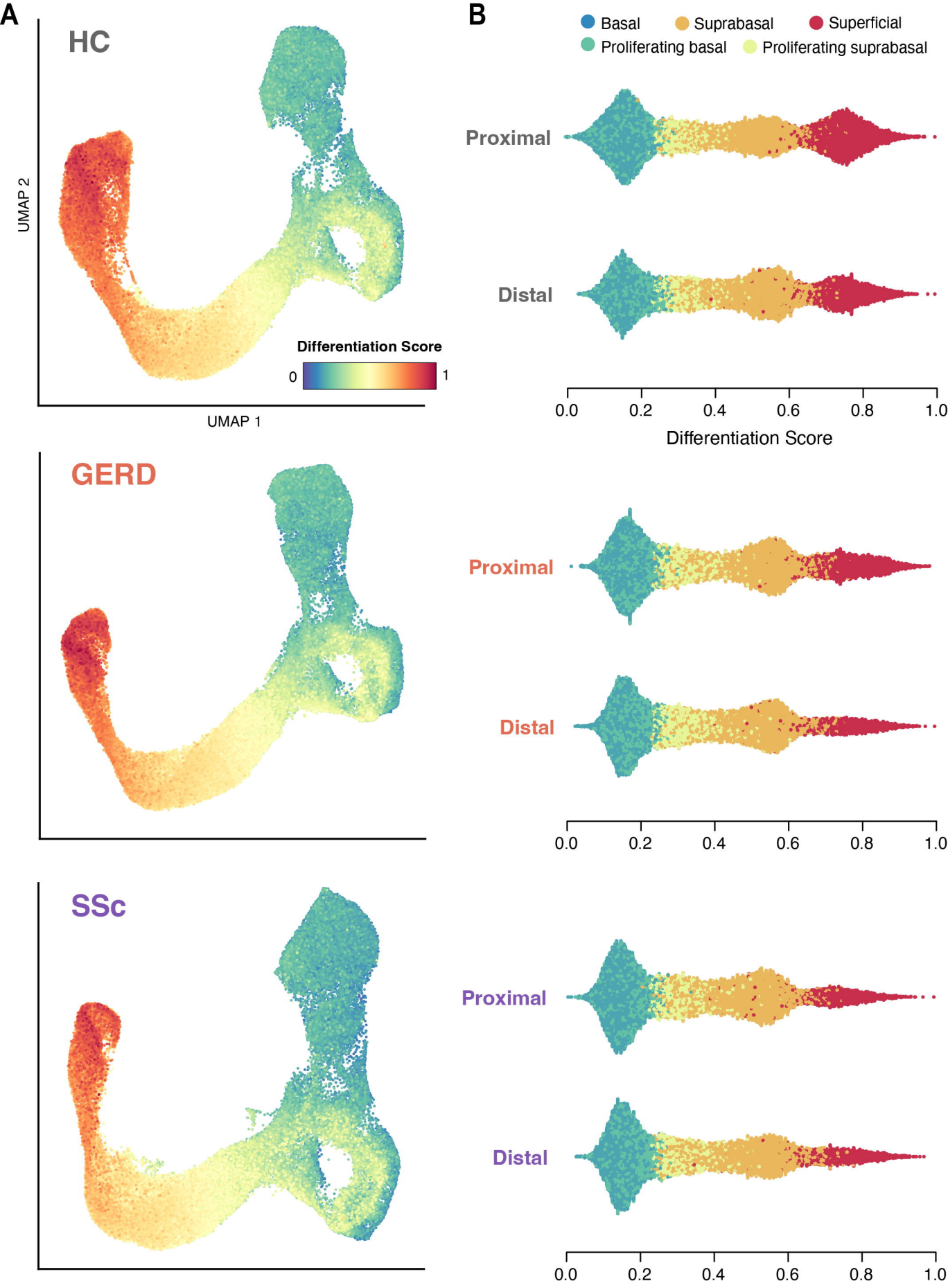
A
HC
UMAP 2
UMAP 1
Differentiation Score
0
1
GERD
SSc
B
Basal
Suprabasal
Superficial
Proliferating basal
Proliferating suprabasal
Proximal
Distal
0.0
0.2
0.4
0.6
0.8
1.0
Differentiation Score

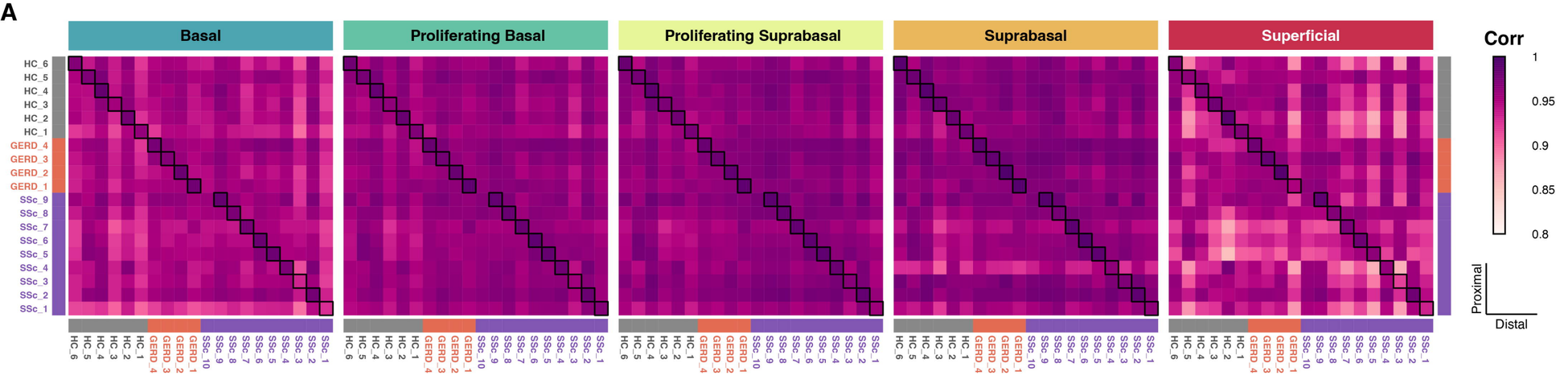

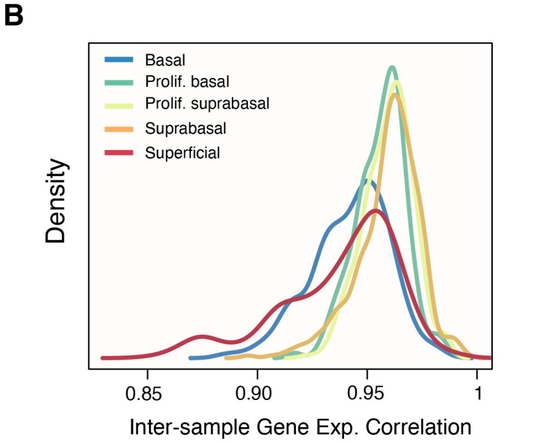

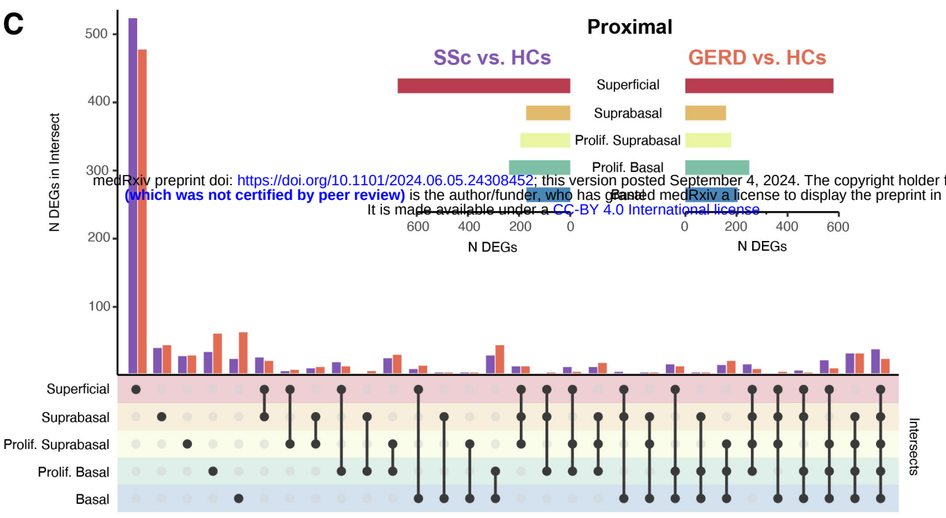

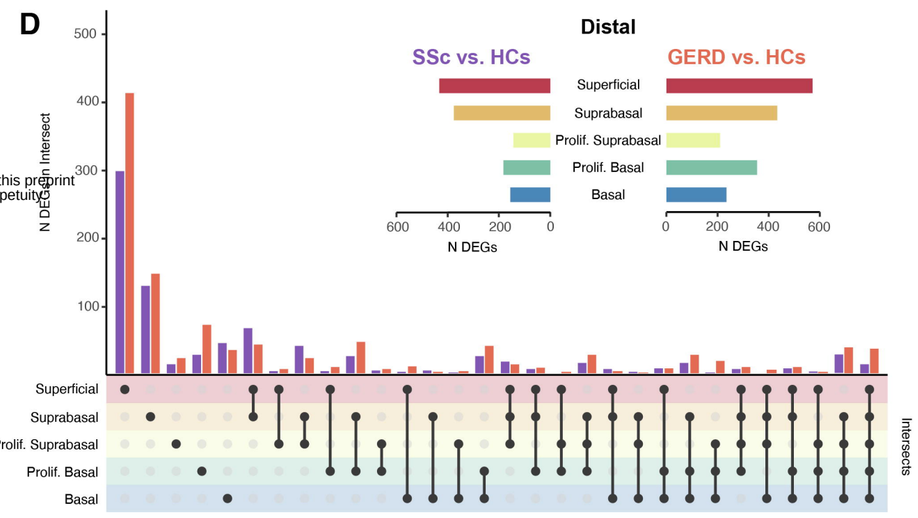

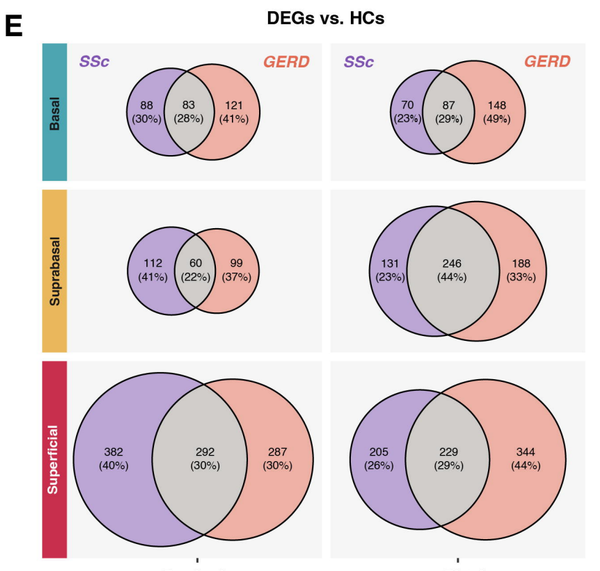

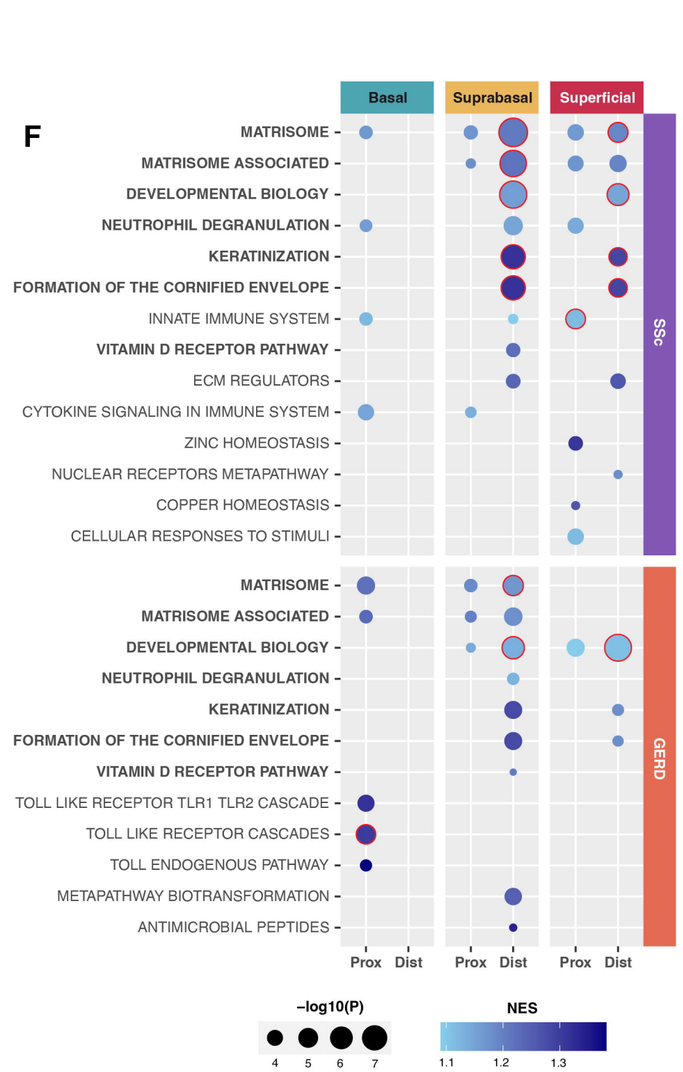

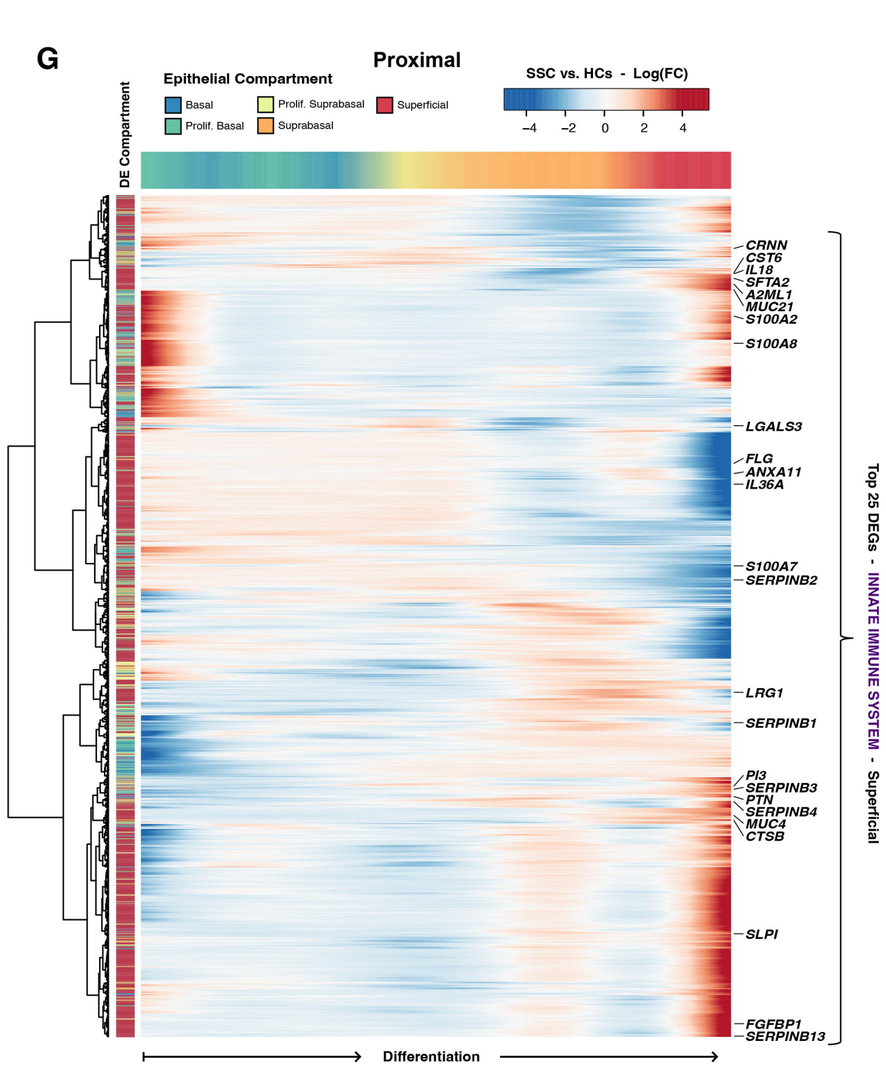

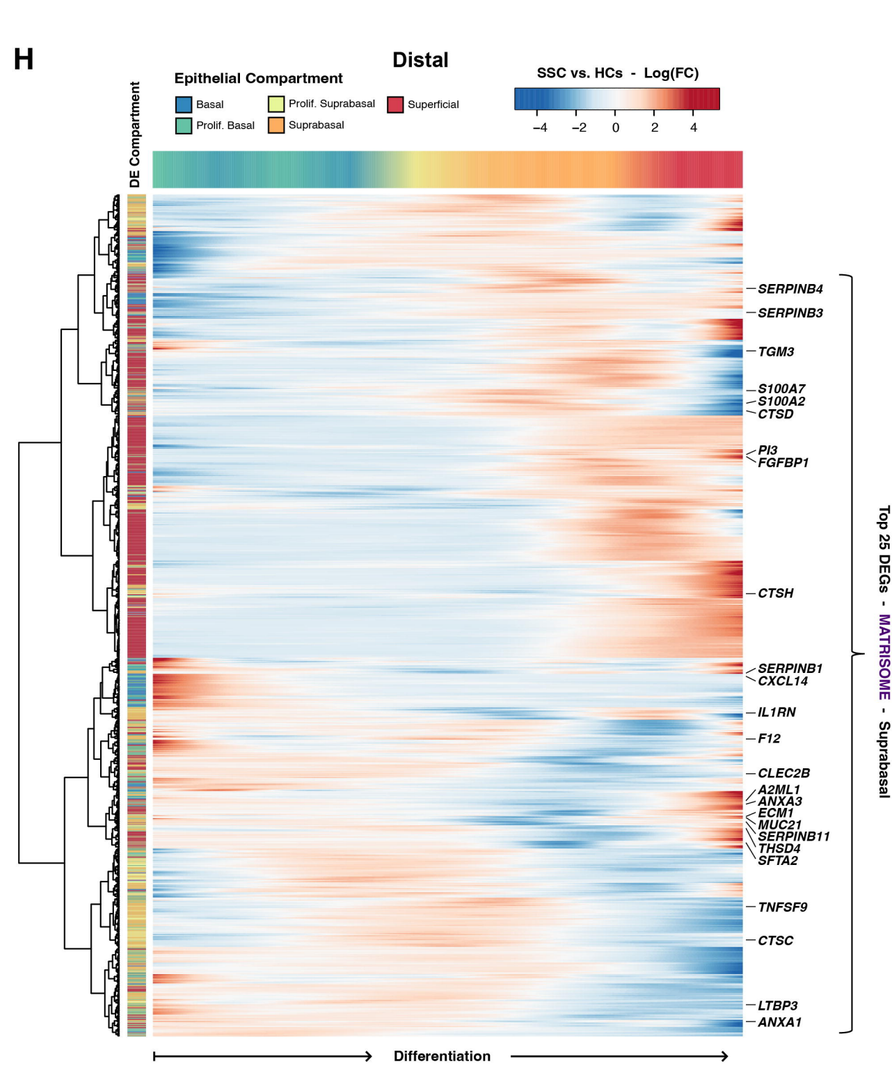

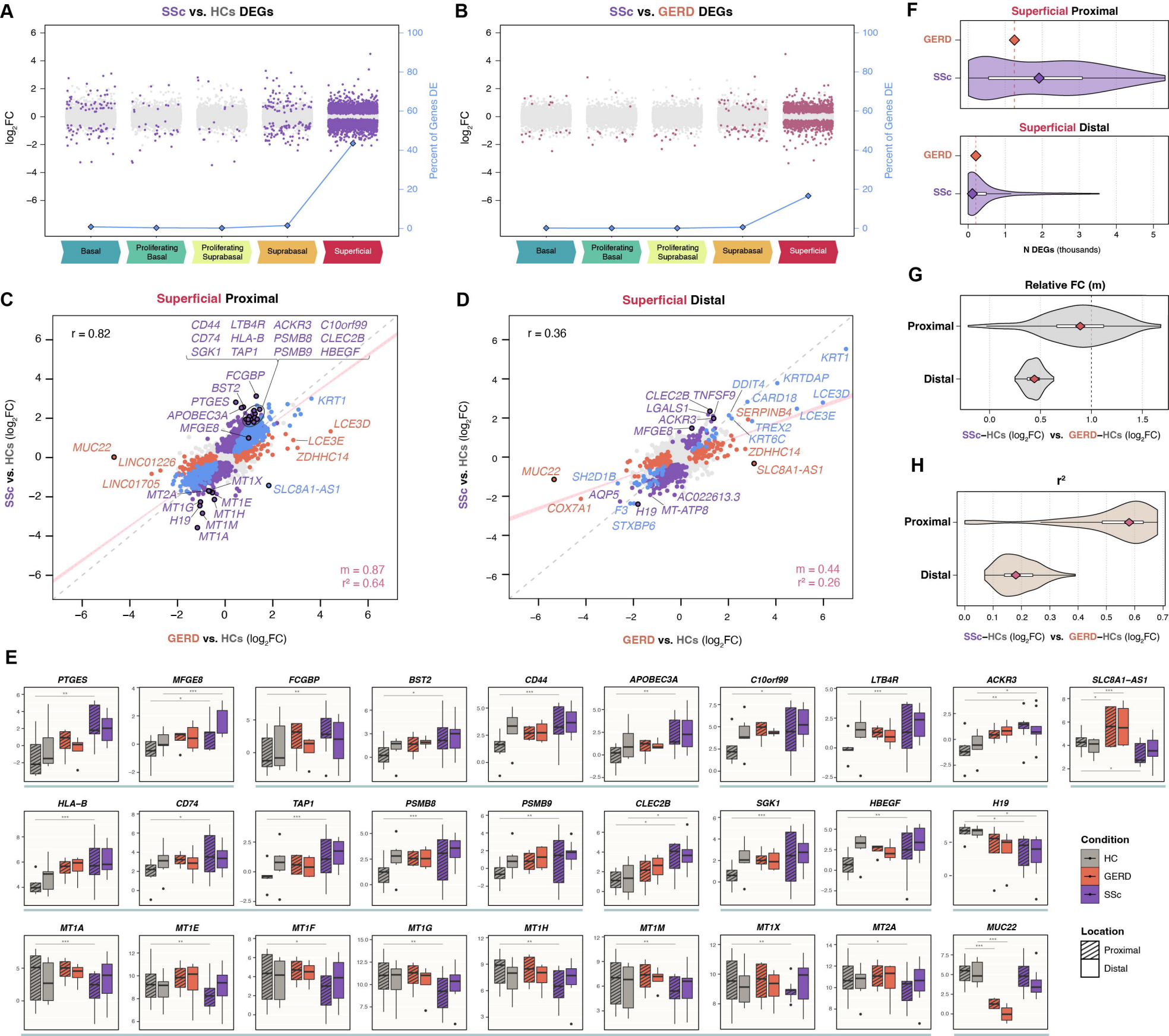
A
SSc vs. HCs DEGs
log2FC
Percent of Genes DE
Basal
Proliferating Basal
Proliferating Suprabasal
Suprabasal
Superficial
B
SSc vs. GERD DEGs
F
Superficial Proximal
GERD
SSc
Superficial Distal
N DEGs (thousands)
G
Relative FC (m)
Proximal
Distal
SSc–HCs (log2FC) vs. GERD–HCs (log2FC)
H
r²
C
Superficial Proximal
r = 0.82
CD44 LTB4R ACKR3 C10orf99
CD74 HLA-B PSMB8 CLEC2B
SGK1 TAP1 PSMB9 HBEGF
FCGBP
BST2
PTGES
APOBEC3A
MFGE8
KRT1
LCE3D
LCE3E
ZDHHC14
MUC22
LINC01226
LINC01705
MT2A
MT1X
SLC8A1-AS1
MT1G
MT1E
MT1H
H19
MT1M
MT1A
m = 0.87
r² = 0.64
SSc vs. HCs (log2FC)
GERD vs. HCs (log2FC)
D
Superficial Distal
r = 0.36
KRT1
DDIT4
KRTDAP
CLEC2B TNFSF9
CARD18
LCE3D
LGALS1
SERPINB4
LCE3E
ACKR3
TREX2
MFGE8
KRT6C
ZDHHC14
SLC8A1-AS1
MUC22
SH2D1B
AQP5
AC022613.3
COX7A1
F3
H19
MT-ATP8
STXBP6
m = 0.44
r² = 0.26
E
PTGES
MFGE8
FCGBP
BST2
CD44
APOBEC3A
C10orf99
LTB4R
ACKR3
SLC8A1–AS1
HLA–B
CD74
TAP1
PSMB8
PSMB9
CLEC2B
SGK1
HBEGF
H19
MT1A
MT1E
MT1F
MT1G
MT1H
MT1M
MT1X
MT2A
MUC22
Condition
HC
GERD
SSc
Location
Proximal
Distal

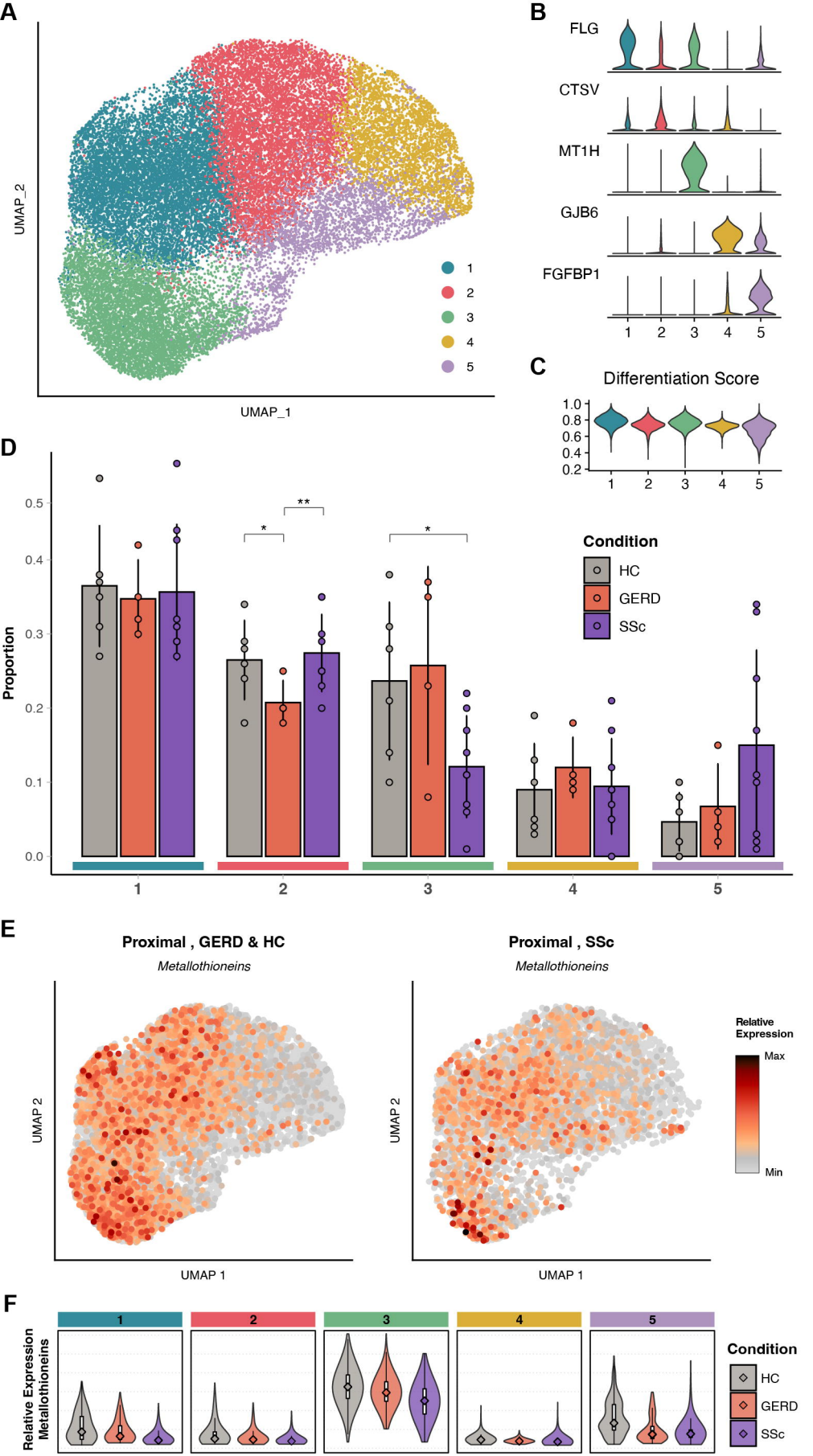
A
UMAP_2
UMAP_1
1
2
3
4
5
B
FLG
CTSV
MT1H
GJB6
FGFBP1
1 2 3 4 5
C
Differentiation Score
1.0
0.8
0.6
0.4
0.2
1 2 3 4 5
D
Proportion
0.5
0.4
0.3
0.2
0.1
0.0
*
**
*
Condition
HC
GERD
SSc
1 2 3 4 5
E
Proximal , GERD & HC
Metallothioneins
Proximal , SSc
Metallothioneins
UMAP 2
UMAP 1
Relative Expression
Max
Min
F
1 2 3 4 5
Relative Expression Metallothioneins
Condition
HC
GERD
SSc

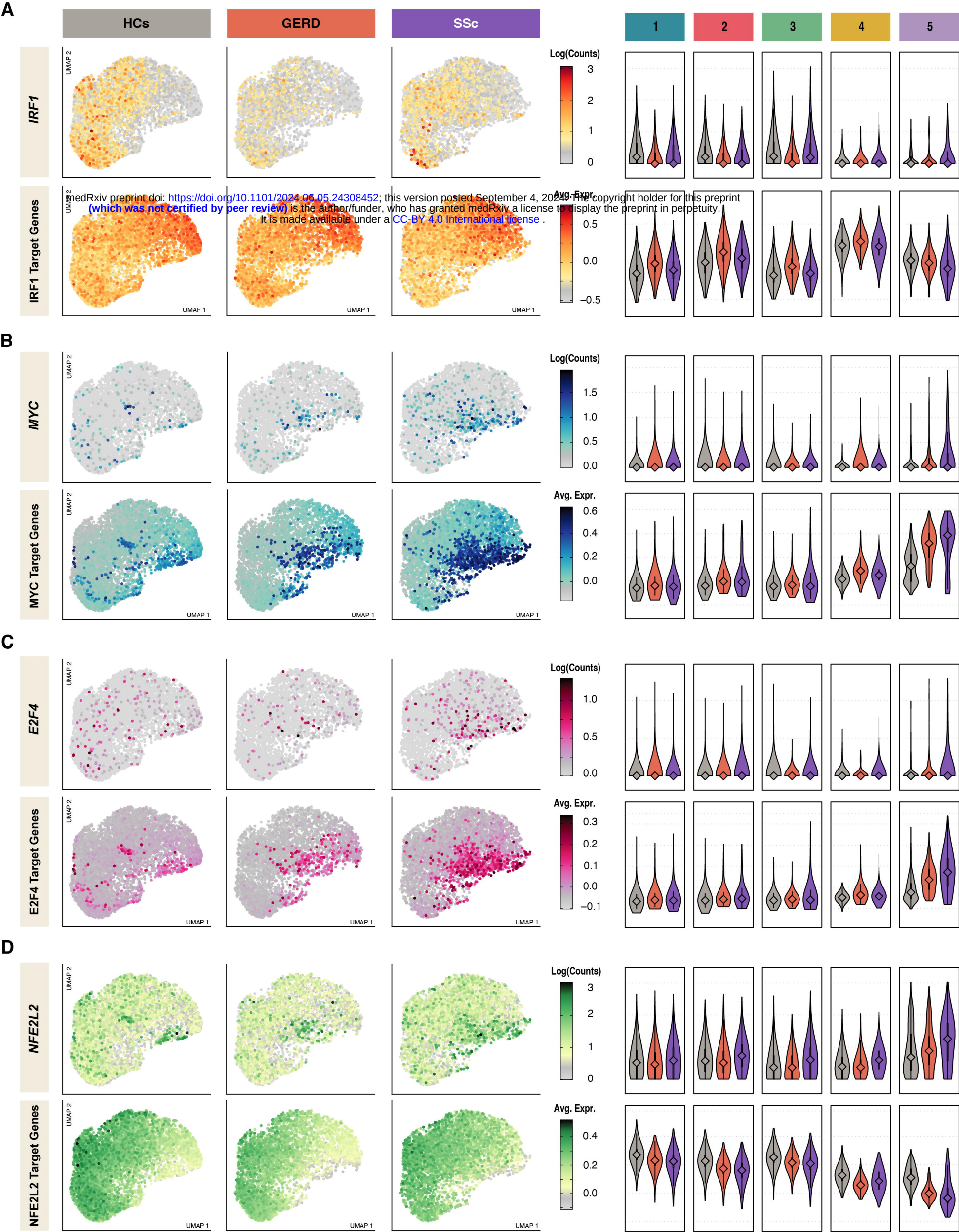

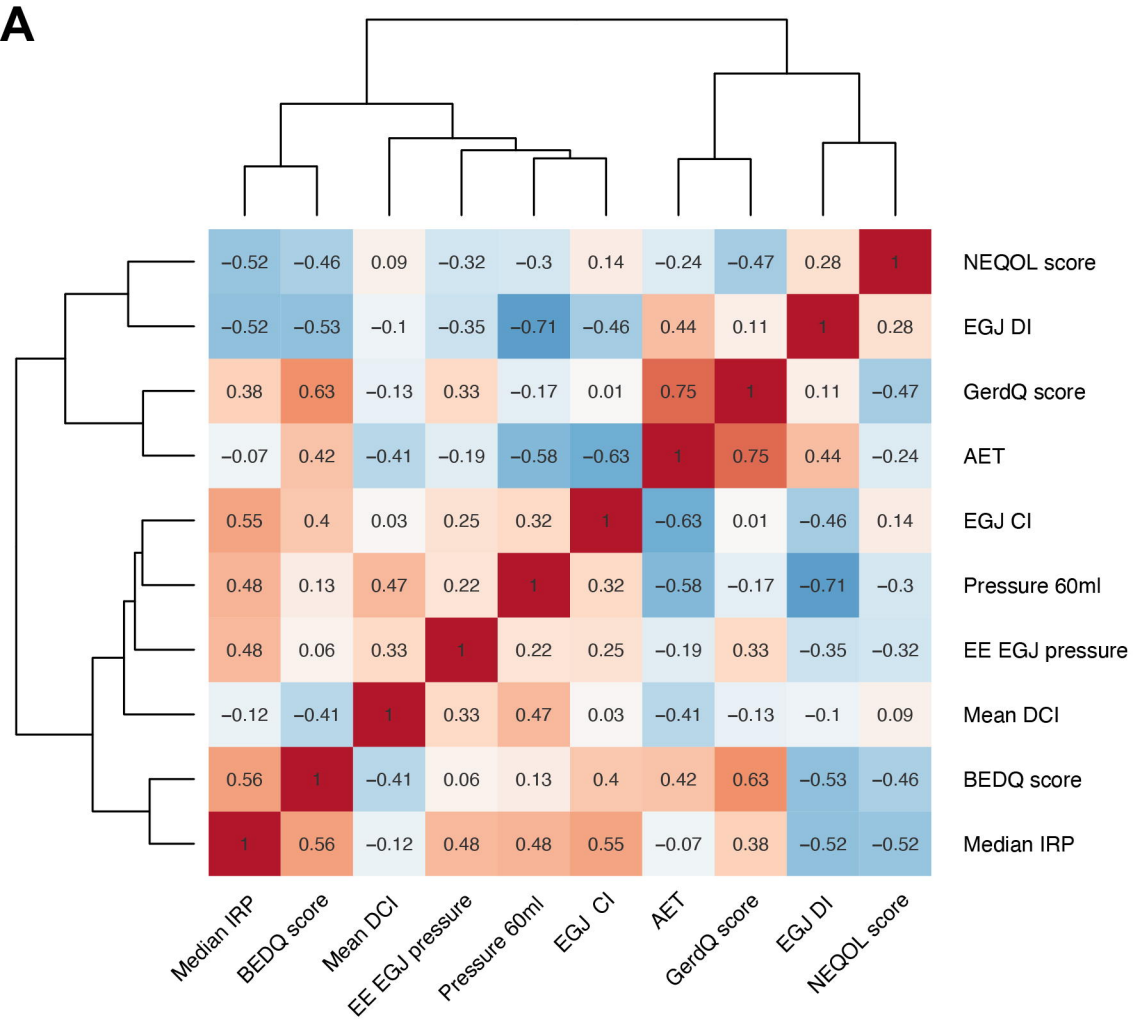

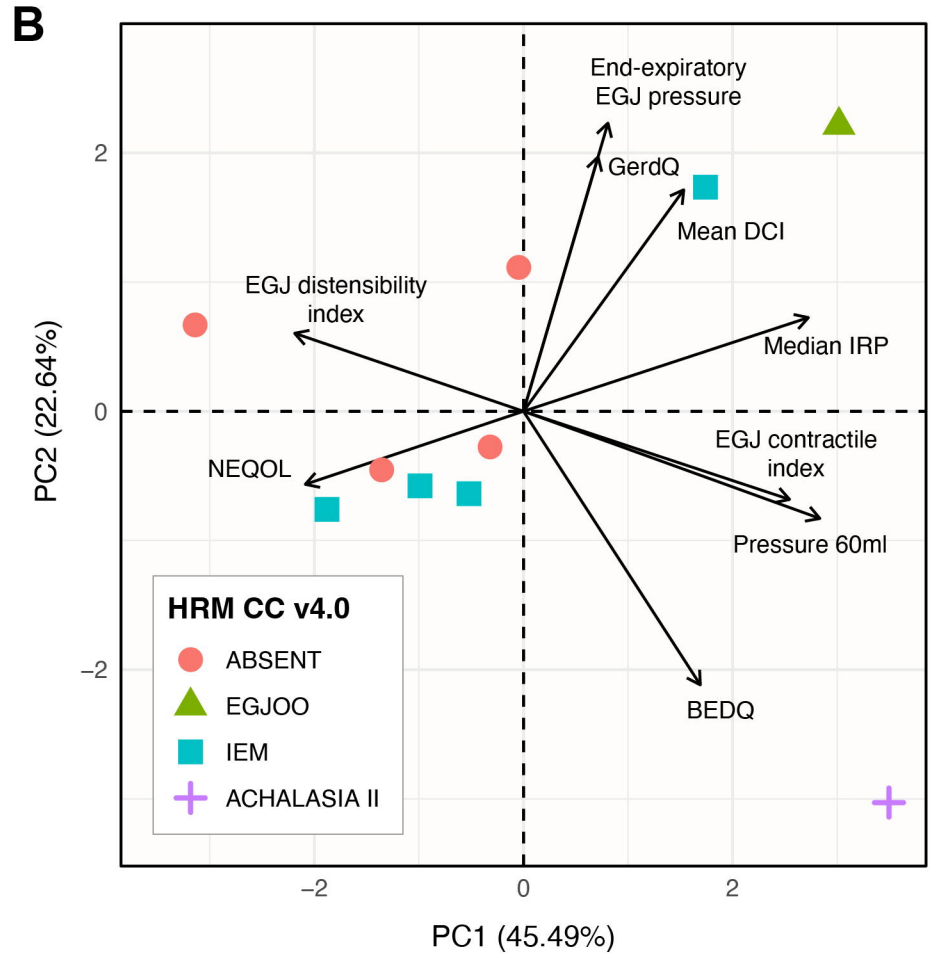

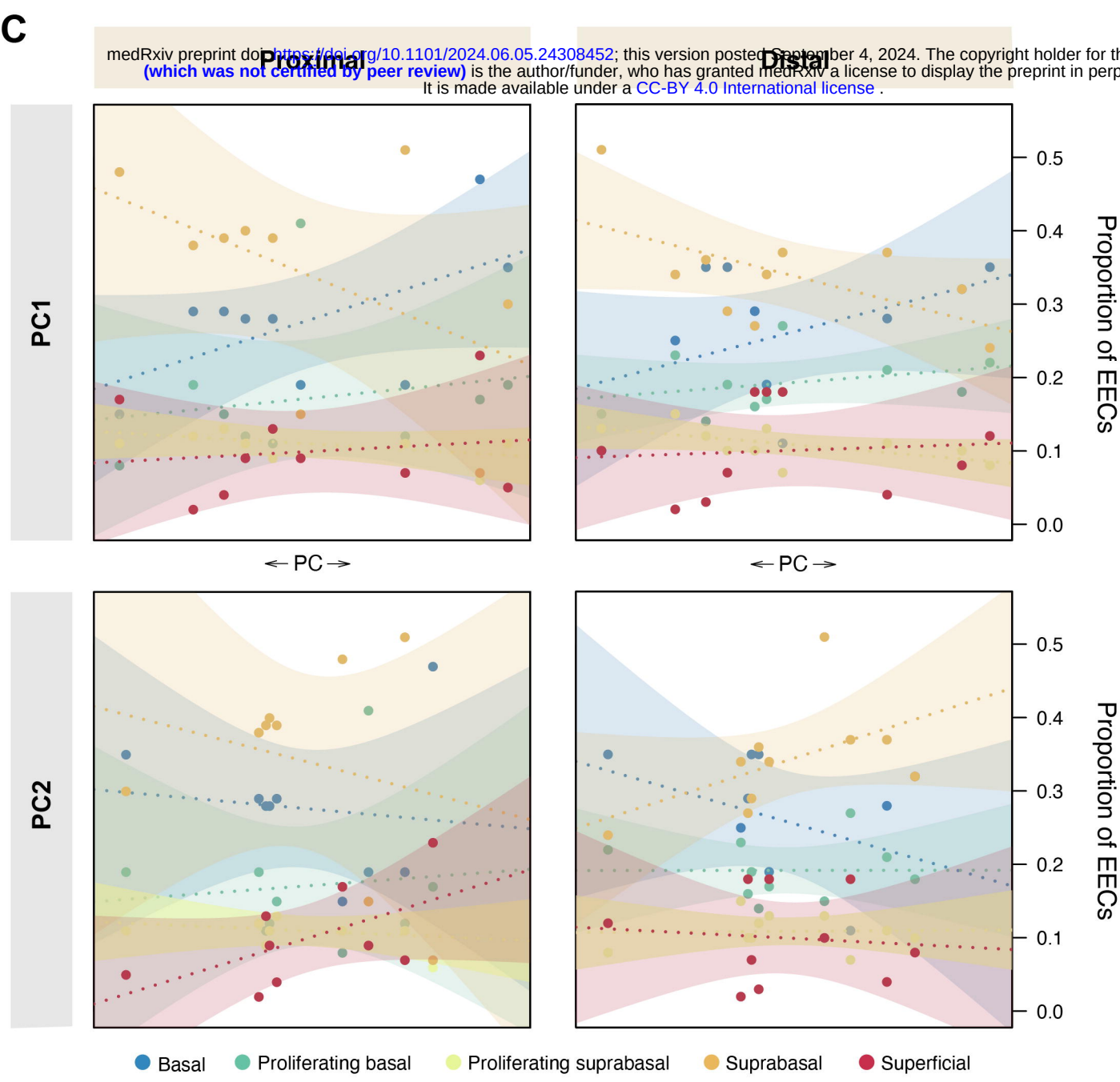

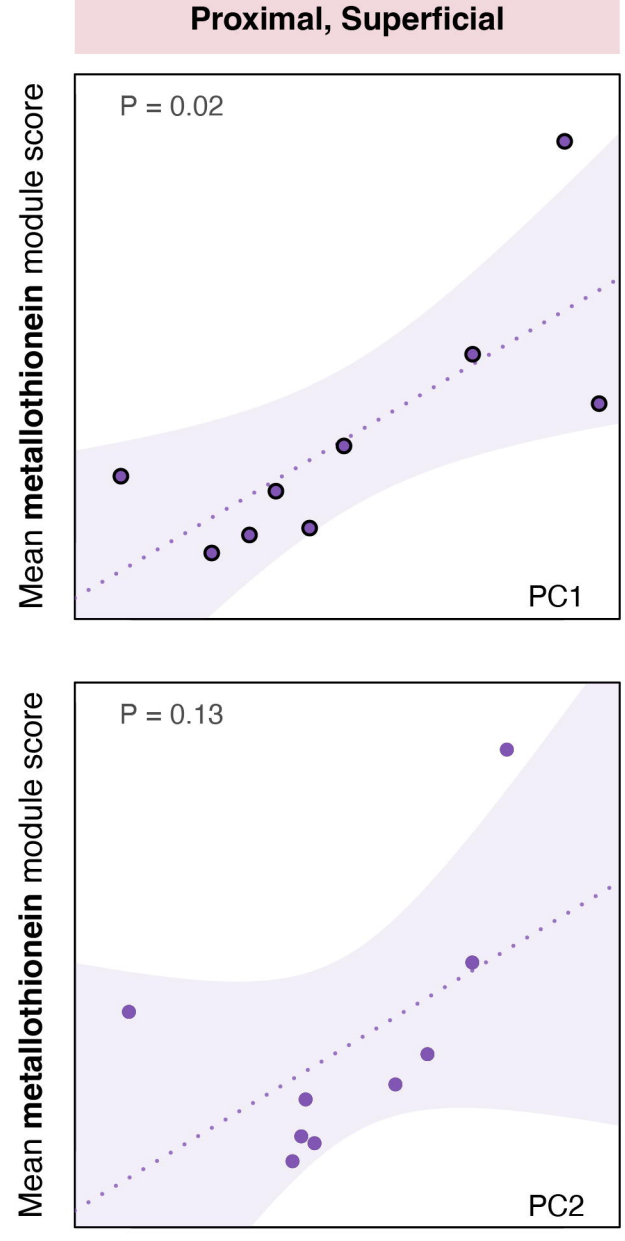

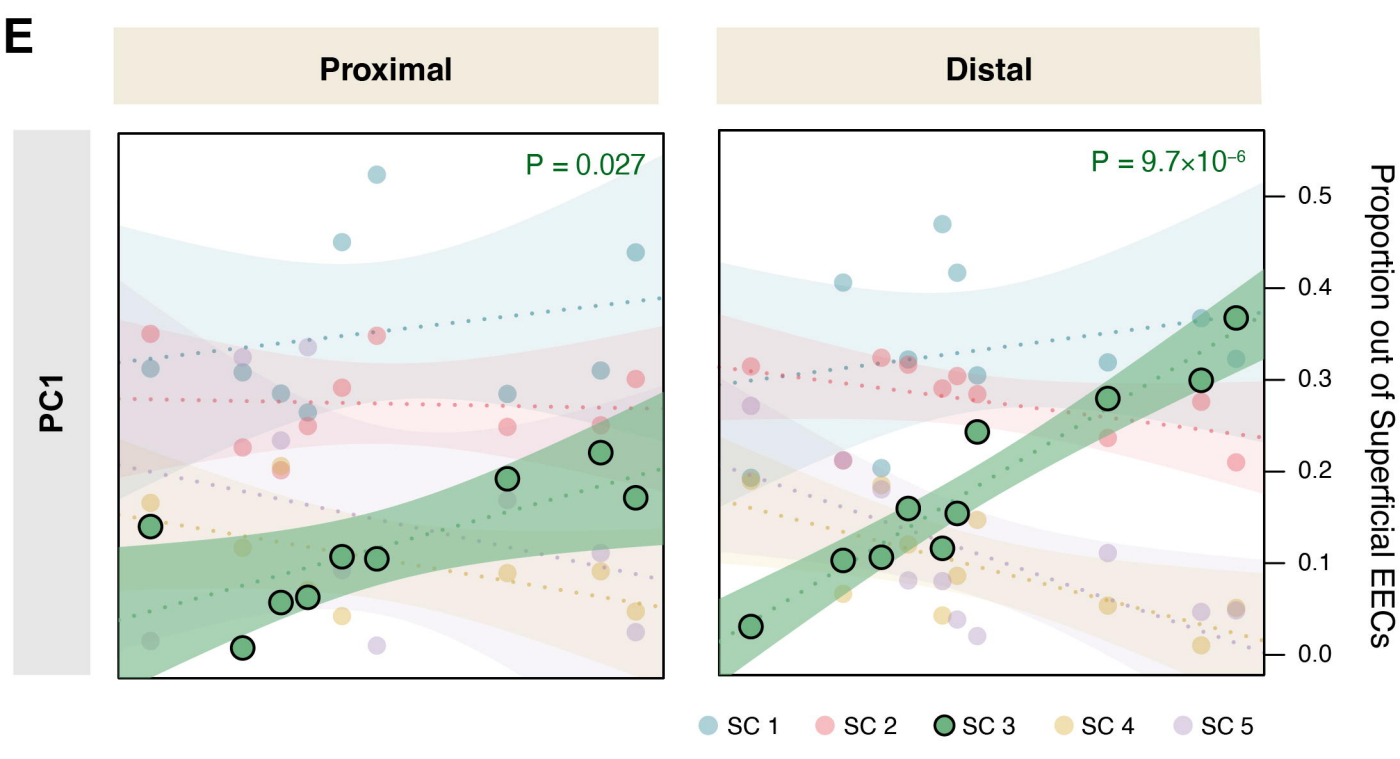

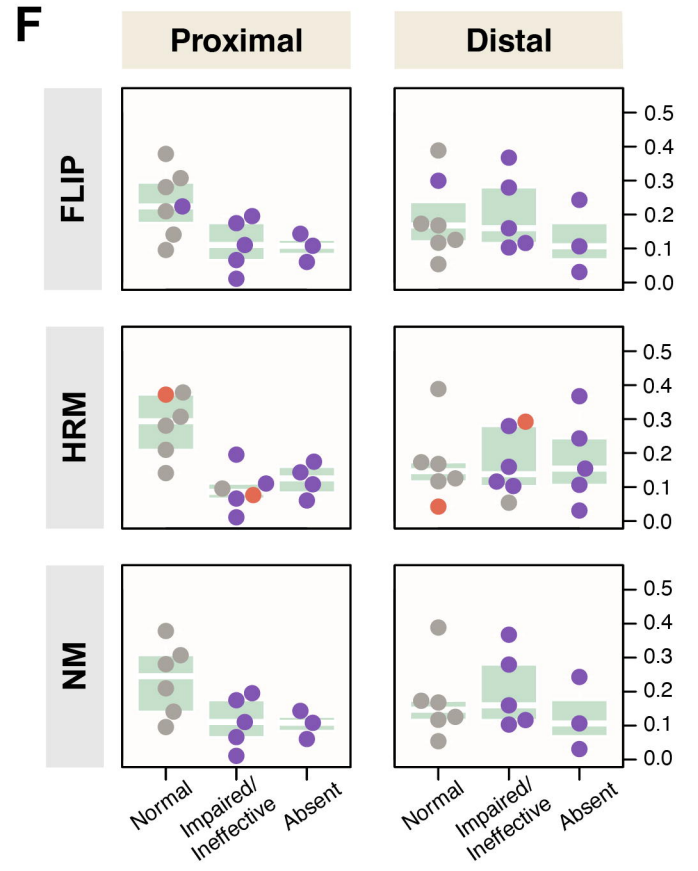

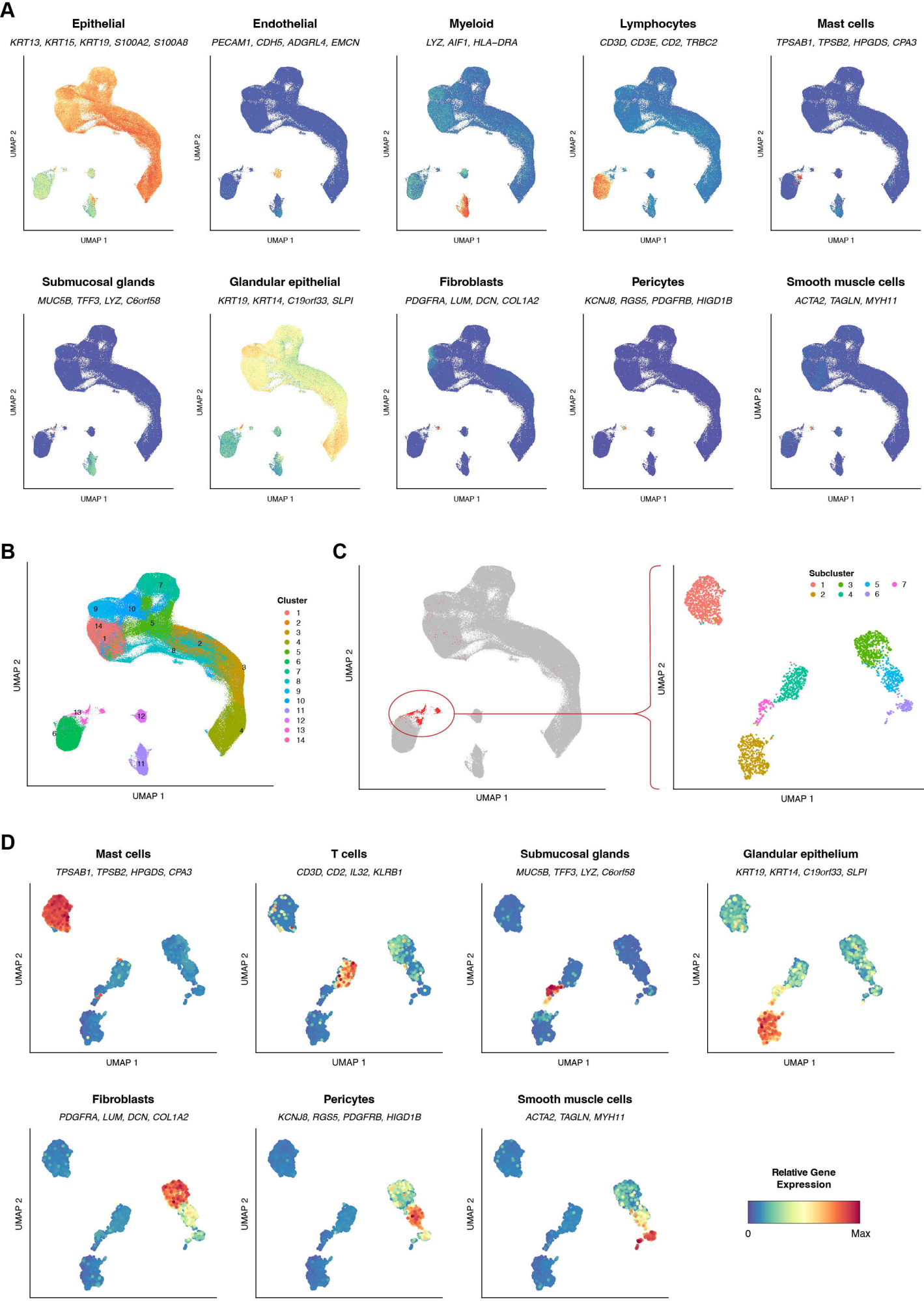
A
Epithelial
KRT13, KRT15, KRT19, S100A2, S100A8
Endothelial
PECAM1, CDH5, ADGRL4, EMCN
Myeloid
LYZ, AIF1, HLA–DRA
Lymphocytes
CD3D, CD3E, CD2, TRBC2
Mast cells
TPSAB1, TPSB2, HPGDS, CPA3
Submucosal glands
MUC5B, TFF3, LYZ, C6orf58
Glandular epithelial
KRT19, KRT14, C19orf33, SLPI
Fibroblasts
PDGFRA, LUM, DCN, COL1A2
Pericytes
KCNJ8, RGS5, PDGFRB, HIGD1B
Smooth muscle cells
ACTA2, TAGLN, MYH11
UMAP 1
UMAP 2
B
Cluster
1
2
3
4
5
6
7
8
9
10
11
12
13
14
C
Subcluster
D
Mast cells
TPSAB1, TPSB2, HPGDS, CPA3
T cells
CD3D, CD2, IL32, KLRB1
Submucosal glands
MUC5B, TFF3, LYZ, C6orf58
Glandular epithelium
KRT19, KRT14, C19orf33, SLPI
Fibroblasts
PDGFRA, LUM, DCN, COL1A2
Pericytes
KCNJ8, RGS5, PDGFRB, HIGD1B
Smooth muscle cells
ACTA2, TAGLN, MYH11
Relative Gene Expression
0
Max

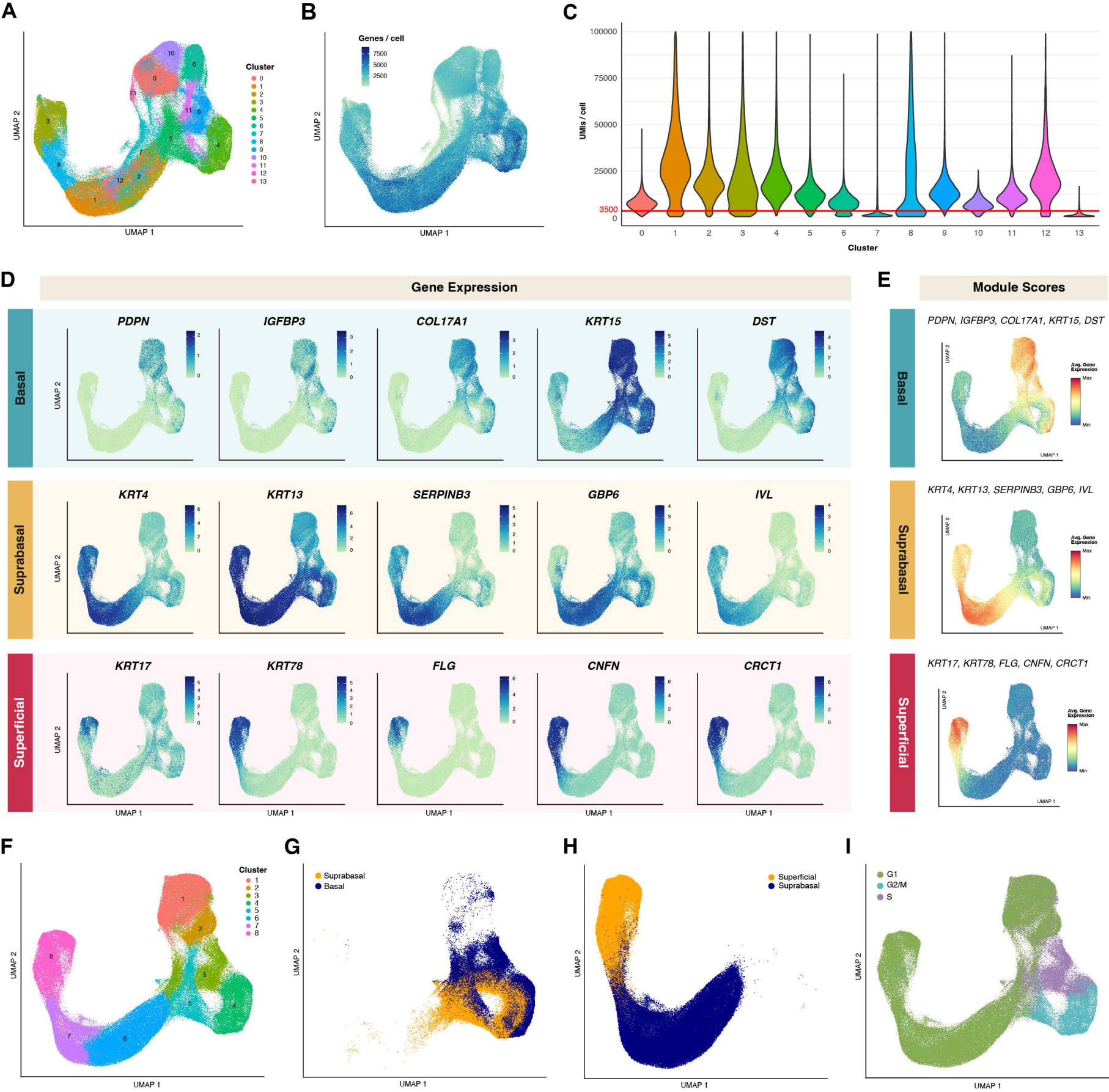
A
B
C
D
E
F
G
H
I
Cluster
Genes / cell
UMIs / cell
UMAP 1
UMAP 2
Gene Expression
Module Scores
Basal
Suprabasal
Superficial
PDPN
IGFBP3
COL17A1
KRT15
DST
KRT4
KRT13
SERPINB3
GBP6
IVL
KRT17
KRT78
FLG
CNFN
CRCT1
PDPN, IGFBP3, COL17A1, KRT15, DST
KRT4, KRT13, SERPINB3, GBP6, IVL
KRT17, KRT78, FLG, CNFN, CRCT1
Avg. Gene Expression
Max
Min
Suprabasal
Basal
Superficial
Suprabasal
G1
G2/M
S

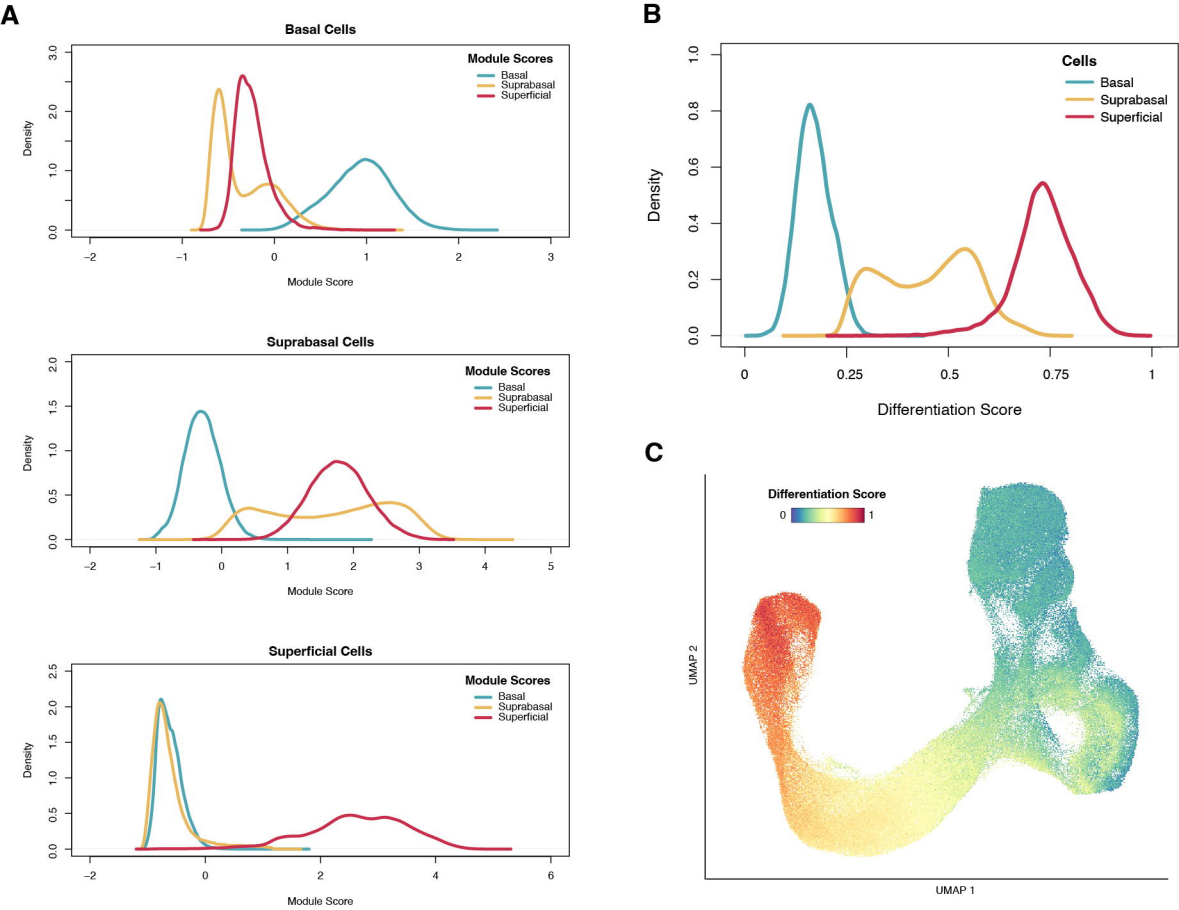
A
Basal Cells
Module Scores
Basal
Suprabasal
Superficial
Density
Module Score
Suprabasal Cells
Module Scores
Basal
Suprabasal
Superficial
Density
Module Score
Superficial Cells
Module Scores
Basal
Suprabasal
Superficial
Density
Module Score
B
Cells
Basal
Suprabasal
Superficial
Density
Differentiation Score
C
Differentiation Score
0
1
UMAP 2
UMAP 1

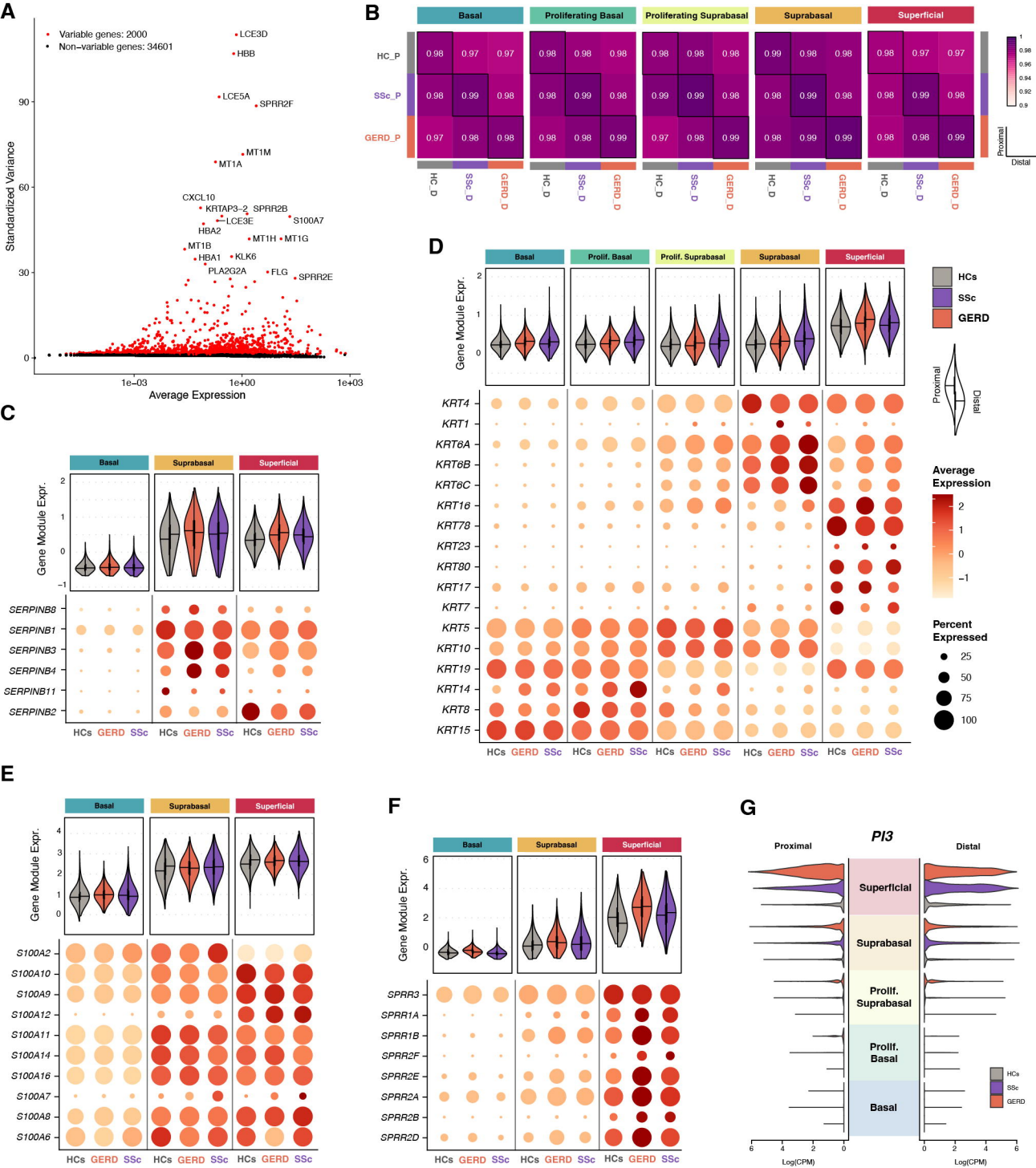
A
Variable genes: 2000
Non−variable genes: 34601
LCE3D
HBB
LCE5A
SPRR2F
MT1M
MT1A
CXCL10
KRTAP3−2
SPRR2B
LCE3E
S100A7
HBA2
MT1H
MT1G
MT1B
HBA1
KLK6
PLA2G2A
FLG
SPRR2E
Standardized Variance
Average Expression
B
Basal
Proliferating Basal
Proliferating Suprabasal
Suprabasal
Superficial
HC_P
SSc_P
GERD_P
HC_D
SSc_D
GERD_D
Proximal
Distal
C
Basal
Suprabasal
Superficial
Gene Module Expr.
SERPINB8
SERPINB1
SERPINB3
SERPINB4
SERPINB11
SERPINB2
HCs GERD SSc
D
Basal
Prolif. Basal
Prolif. Suprabasal
Suprabasal
Superficial
Gene Module Expr.
KRT4
KRT1
KRT6A
KRT6B
KRT6C
KRT16
KRT78
KRT23
KRT80
KRT17
KRT7
KRT5
KRT10
KRT19
KRT14
KRT8
KRT15
HCs
SSc
GERD
Proximal
Distal
Average Expression
Percent Expressed
25
50
75
100
E
Basal
Suprabasal
Superficial
Gene Module Expr.
S100A2
S100A10
S100A9
S100A12
S100A11
S100A14
S100A16
S100A7
S100A8
S100A6
HCs GERD SSc
F
Basal
Suprabasal
Superficial
Gene Module Expr.
SPRR3
SPRR1A
SPRR1B
SPRR2F
SPRR2E
SPRR2A
SPRR2B
SPRR2D
HCs GERD SSc
G
PI3
Proximal
Distal
Superficial
Suprabasal
Prolif. Suprabasal
Prolif. Basal
Basal
HCs
SSc
GERD
Log(CPM)
Log(CPM)

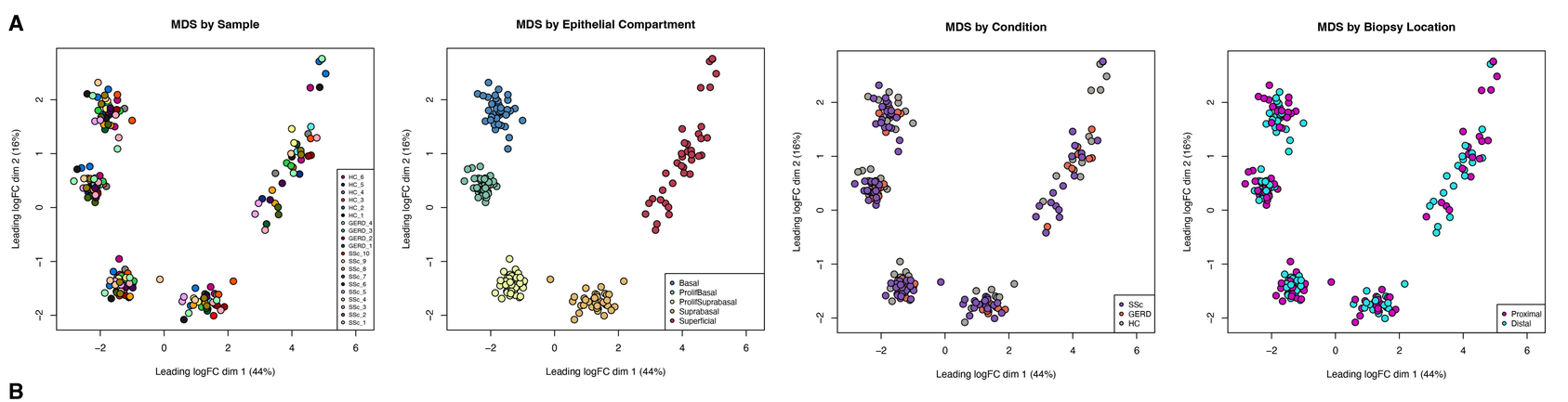

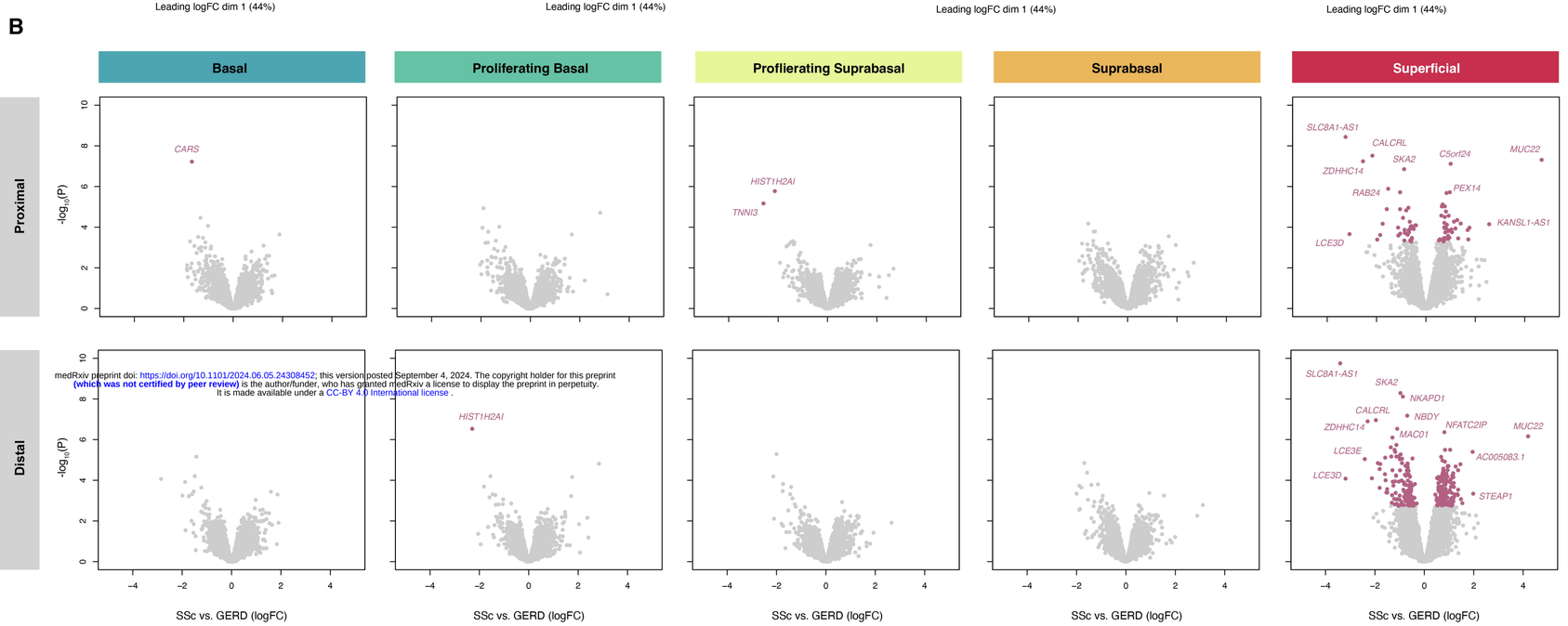

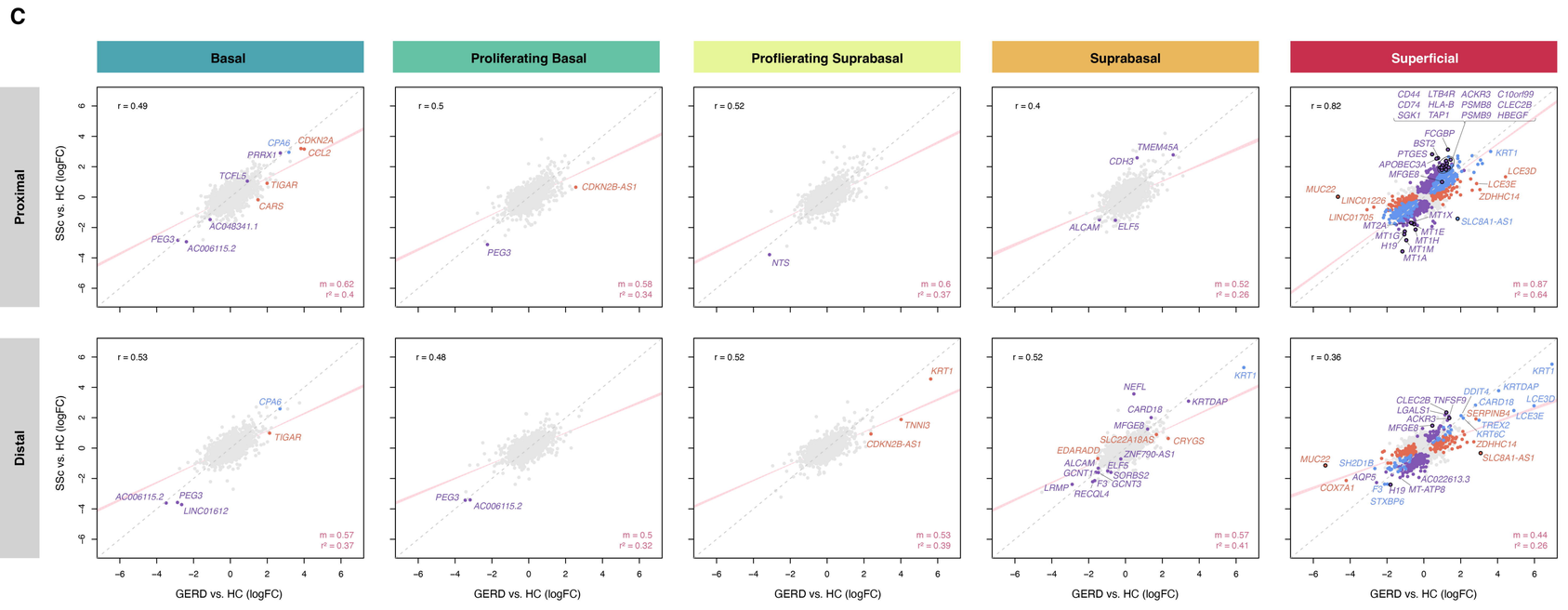

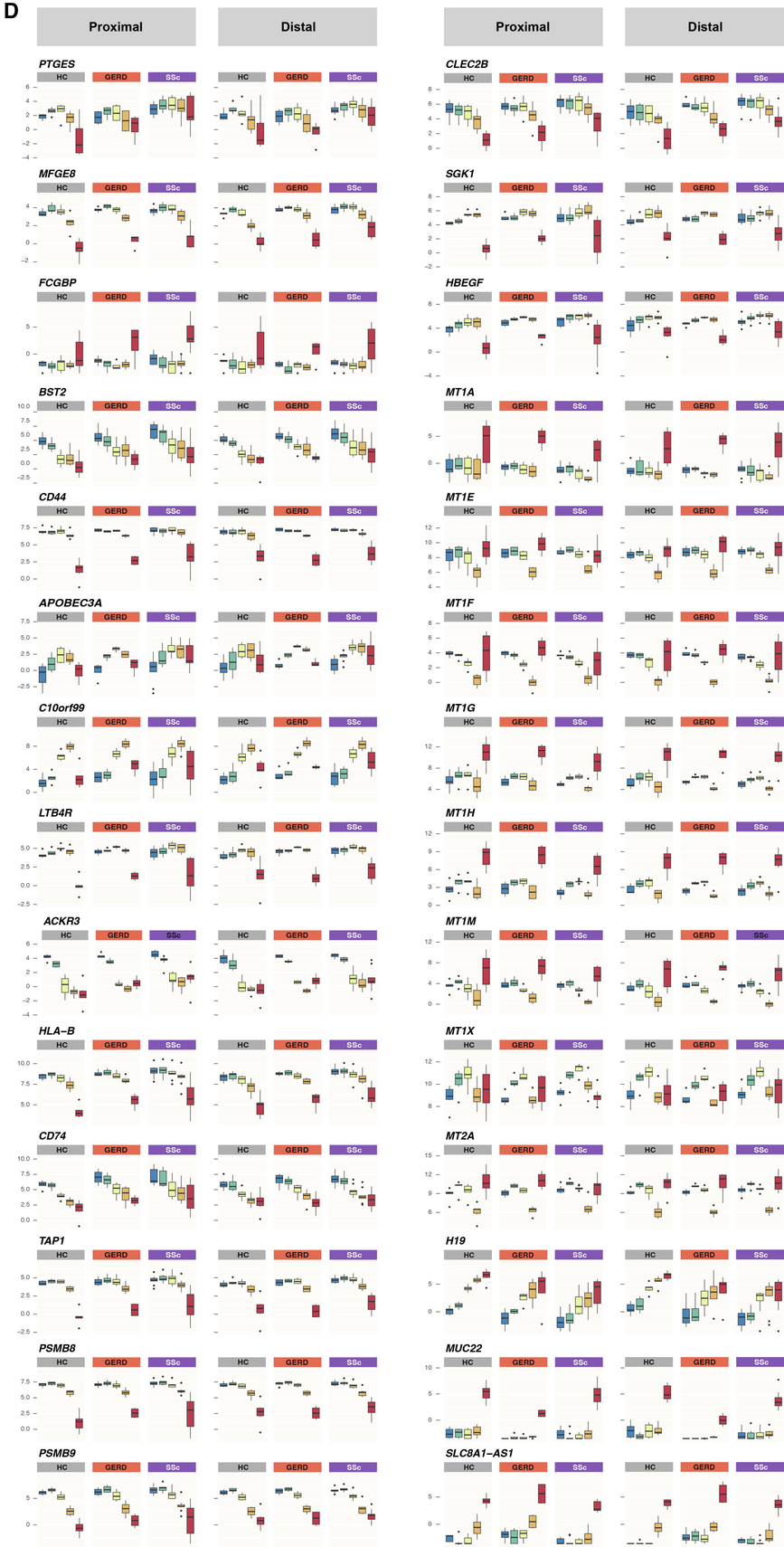

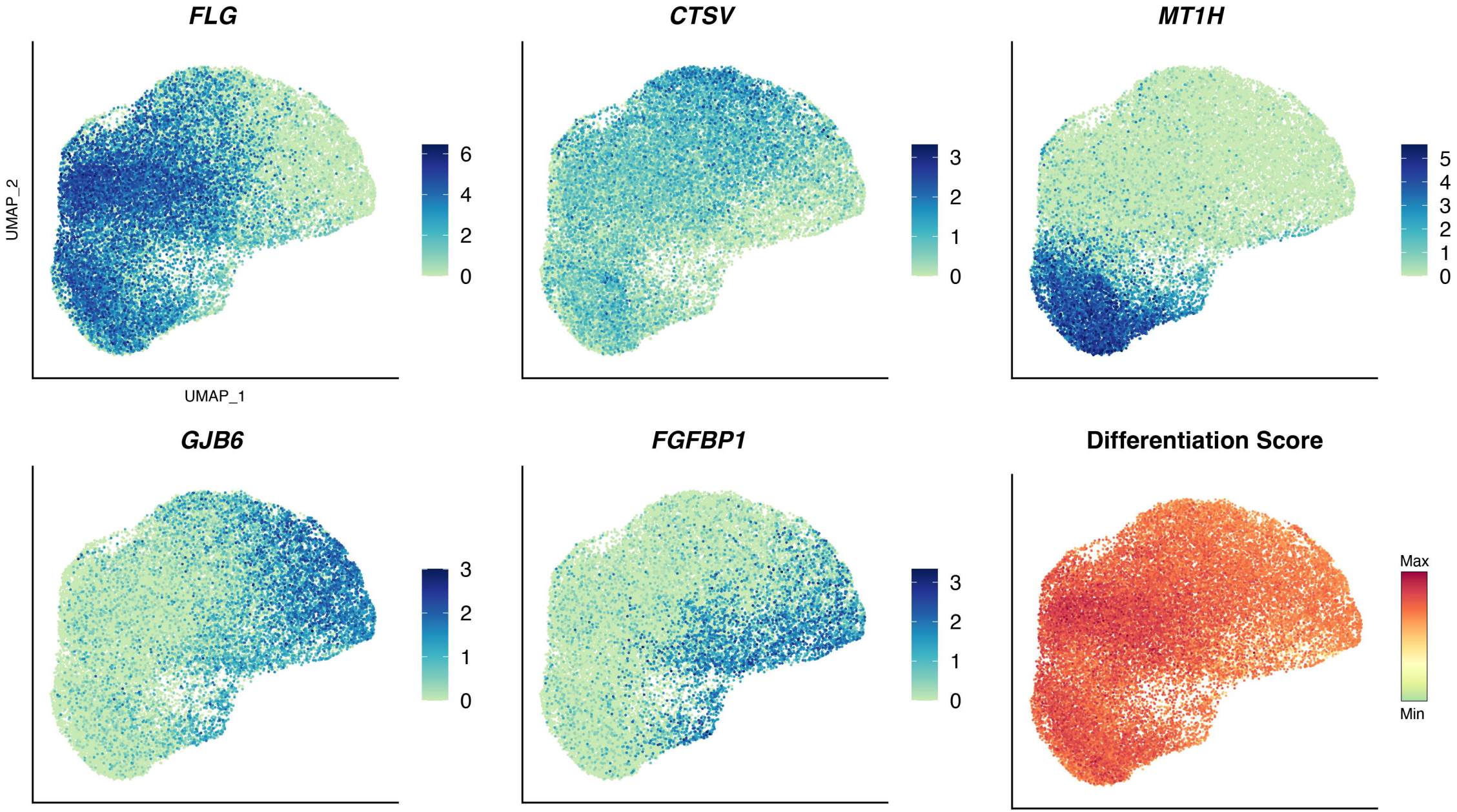
FLG
CTSV
MT1H
GJB6
FGFBP1
Differentiation Score
UMAP_2
UMAP_1
6
4
2
0
3
2
1
0
5
4
3
2
1
0
3
2
1
0
3
2
1
0
Max
Min

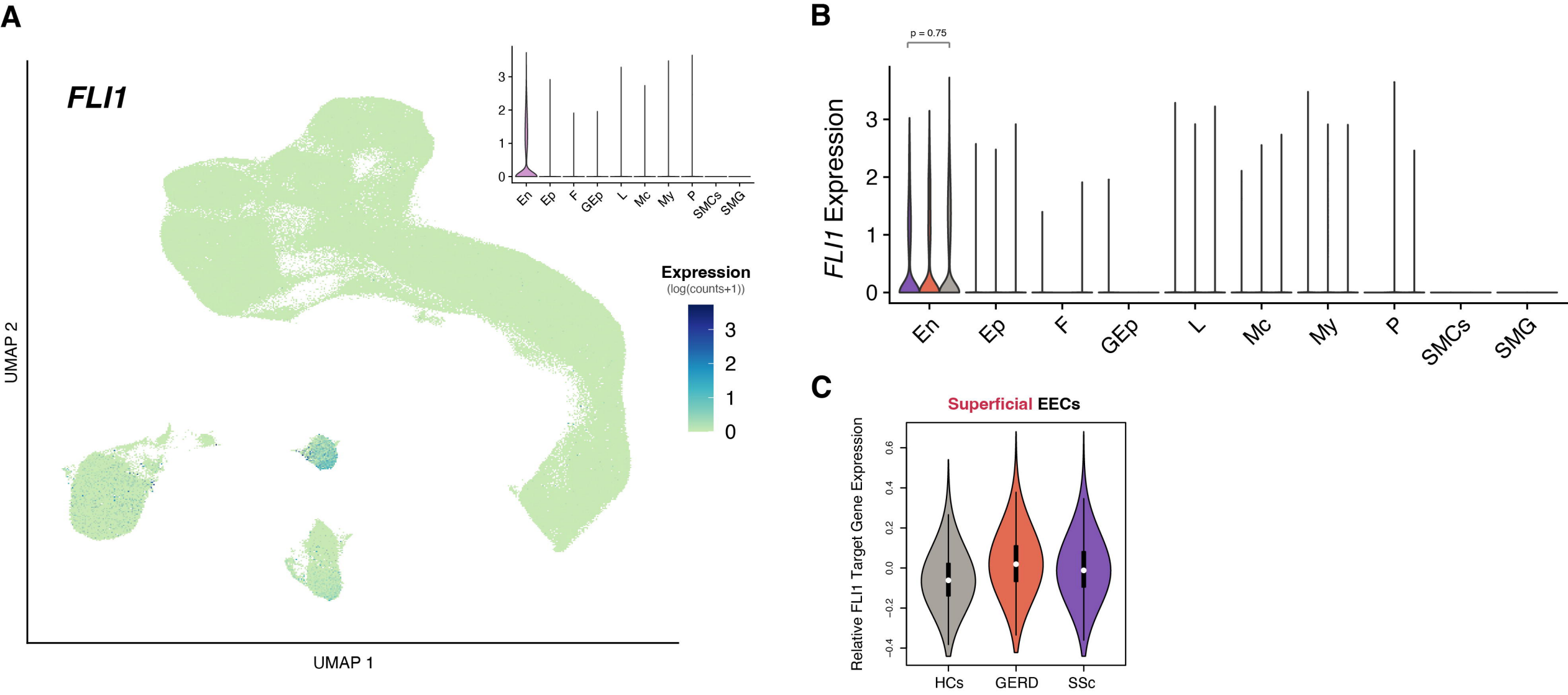
A
FLI1
UMAP 2
UMAP 1
Expression
(log(counts+1))
3
2
1
0
En
Ep
F
GEp
L
Mc
My
P
SMCs
SMG
B
p = 0.75
FLI1 Expression
C
Superficial EECs
Relative FLI1 Target Gene Expression
HCs
GERD
SSc